Movement Resistant Orientation Selective Neurons in the Deep Layers of the Rat Primary Visual Cortex

Master thesis in Molecular Biosciences

Main field in physiology and neurobiology

Malin Benum Røe

60 credits

Program for Physiology and Neurobiology

Department of Biosciences

The Faculty of Mathematics and Natural Sciences

UNIVERSITY OF OSLO

September 2016

Movement Resistant Orientation Selective Neurons in the Deep Layers of the Rat Primary Visual Cortex

Malin Benum Røe

Program for Physiology and Neurobiology

Department of Biosciences

University of Oslo

September 2016

2016

Movement resistant orientation selective neurons in the deep layers of the rat primary visual cortex

Malin Benum Røe

http://www.duo.uio.no/

Trykk: Reprosentralen, Universitetet i Oslo

Acknowledgements

The work presented in this thesis was conducted at the Program for Physiology and Neurobiology at the Department of Biosciences, University of Oslo between January 2014 and September 2016, under the supervision of associate professors Marianne Fyhn and Torkel Hafting, PhD student Ida E.J. Aasebø and PhD student Kristian K. Lensjø.

First and foremost, I would like to express my gratitude towards my main supervisor Marianne for offering me the opportunity to be a master student in your research group. Thank you for all your help with the writing and guidance along the way, and for being a true inspiration through your passion and accomplishments in the neuroscience field.

I especially want to thank Kristian whose help and support throughout this thesis has been invaluable. I truly appreciate your contagious work ethics and admire the enthusiasm and dedication you show to both the group and your research. Thanks to Ida for introducing me to the intriguing neurons which are the focus of my thesis. You have put up with numerous questions, and have been extremely patient and humble with me not always understanding, which I am grateful for. Thank you both for all the guidance and support with experiments, analysis and writing throughout my thesis which have helped set high standards and encouraged me to work harder. I would also like to thank Torkel for his help with the project and for sharing his knowledge and support over the course of my thesis.

Thank you to all the members of the Hafting-Fyhn lab and associated groups for creating a great educational and social environment that I have felt lucky to be part of.

A special thanks to my fellow students and good friends Heidrun, Marte and Mette for five wonderful years of good memories as well as shared frustrations. It wouldn't have been the same without you. Lastly, I would like to thank my dear Nicholas, mamma and pappa for showing unconditional love and compassion when I needed it the most.

Oslo, September 2016

Malin Benum Røe

Abstract

Neurons in primary visual cortex (V1) respond selectively to visual stimulation of a specific orientation. However, the majority of recordings have been conducted in anesthetized or head-fixed animals excluding the effects of body position and movement on visual processing. In the present study, we addressed this and used chronically implanted tetrodes into the deep layers of V1 to record from single units during visual stimulation in freely moving rats. The specific connectivity of these deep cell layers with reciprocal connections to the thalamus make them uniquely positioned to modulate incoming visual input, and recent preliminary findings from our research groups show neurons with remarkable movement resistant response patterns in these cell layers. In the present study, I followed up these investigations with comprehensive recordings to map out functional characteristics, distribution and population code of neurons in the deep layers of V1.

Most units with orientation tuning were sharply tuned when the animal was sessile but showed a pronounced reduction or complete disruption of orientation selectivity during self-motion. However, a subset of neurons recorded mainly from layer 6 showed remarkably stable orientation selectivity illustrated by their sharp tuning curves and high orientation selectivity index (OSI) values in both states. These movement resistant orientation selective (MROS) neurons displayed minor increases in firing activity during movement with no effect on the preferred orientations of the unit, and only a small reduction in OSI. In contrast, the increased firing activity reduced the orientation selectivity in other orientation selective neurons as the general increase was not confined to preferred orientations. The orientation selectivity of layer 6 neurons and in particular the MROS units were highly reproducible across many trials despite large variations in the animal's movement.

The remarkable orientation tuning stability of this deep layer subpopulation of neurons and their anatomical positioning indicate that they are part of a network compensating for changes in the visual field as a result of head and body movements. The findings from these investigations open for new experimental approaches to reveal the involvement of other brain regions in these processes such as the reciprocal connections to thalamic nuclei like the dLGN or other areas like the vestibular system or brain stem motor areas. Moreover, my findings have implications for theoretical models on the workings of visual information processing.

Table of contents

1 Introduction

Our perception of the world is based on the information we receive from our sensory organs concerning our surroundings. This information is transmitted as electrical signals between neurons of different brain areas, and the contribution of all signals is what ultimately leads to us seeing. By following the visual pathway from sensory receptors in the eye to the thalamus and further to the visual cortex it has been possible to understand how visual information is processed in a stepwise manner and reveal general principles about how the brain is operating. Descriptions regarding basic principles of visual processing, architecture and circuitry described in the following sections concerning the primary visual pathway and the primary visual cortex are based on textbooks from Kandel and co-workers (2013) and Purves and coworkers (2012) as well as reviews from Callaway (1998), Sillito and co-workers (2006), Thompson (2010) and Harris & Sheperd (2015).

1.1 Visual processing

1.1.1 The primary visual pathway

The most studied component of the visual system is the primary visual pathway (Figure 1.1). Over the past decades, it has become clear that even though the primary visual pathway is an early stage of visual processing, it is not synonymous with a simple system, and damage to this pathway can result in serious visual impairments. The visual processing starts at the retina when light activates photoreceptors. The signal is transferred via the ganglion cell axons that bundles together in what is called the optic nerve. The optic nerve from each eye intersect at the optic chiasm where around half of the retinal ganglion cell axons cross over to the opposite side of the brain. The visual information is thereafter sent to the lateral geniculate nucleus (LGN) in the thalamus via the optic tract. The LGN has often been looked upon as a relay center for information processing, and the summation of the signals in the LGN determine what finally ends up in the primary visual cortex (V1). In species less complex than primates, the LGN is differently organized and the retinal input area is termed the dorsal lateral geniculate nucleus (dLGN). The primary visual pathway terminates in V1 which is located in the occipital lobe at the very back of the head. From there the signal is transferred to higher cortical areas via two separate pathways. One is called the dorsal stream and deals

with the spatial aspects of vision, whereas the other is the ventral stream and is important for object recognition and high-resolution forms of vision. The dorsal stream terminates in the parietal lobe and the ventral stream in the temporal lobe. In addition to the dorsal and ventral streams, neurons in the primary visual pathway send collaterals to numerous areas and are reciprocally connected to both nearby and distant brain locations. All these interconnections imply that information ending up in higher visual areas for perception has undergone comprehensive processing before it arrives. In the following section, areas outside the primary visual pathway that is known or speculated to be part of visual processing, will be discussed.

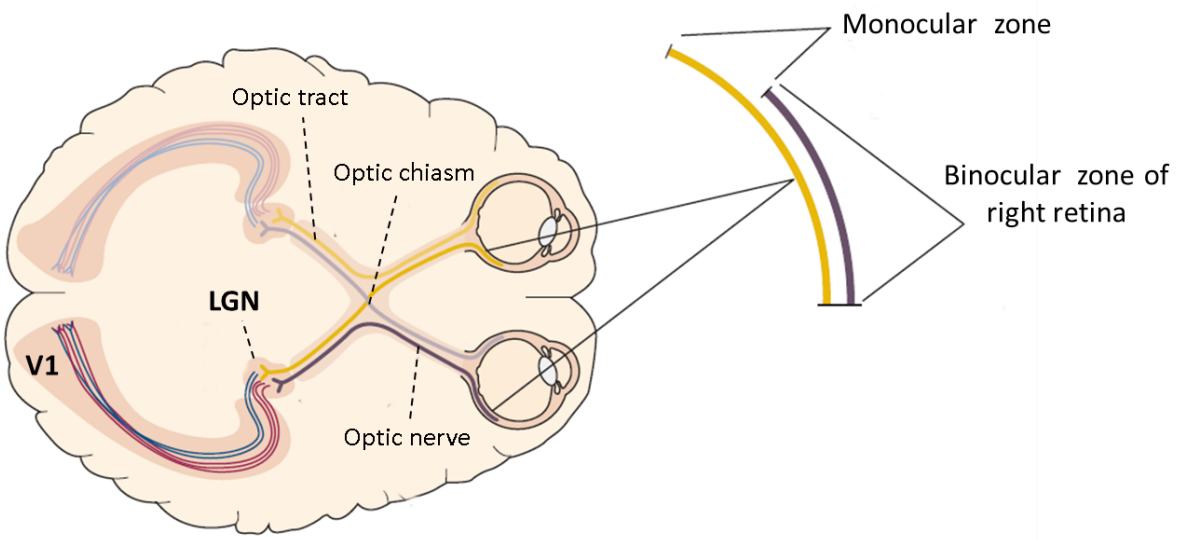

Figure 1.1: The primary visual pathway. The photoreceptors in the retina transduce light into electrical signals that are transferred via retinal ganglion cell axons in the optic nerve to the optic chiasm. Around half of the retinal ganglion cell axons cross in the optic chiasm and proceed in the optic tract on the ipsilateral side. The retinal ganglion cells terminate in the lateral geniculate nucleus (LGN), which transmit the visual information to the primary visual cortex (V1). Modified from Figure 25.12 (Kandel et al., 2013).

1.1.2 Visual processing outside the primary visual pathway

Visual processing does not start and end with the primary visual pathway and the dorsal and ventral stream. Retinal ganglion cells also project to multiple subdivisions of the brain by direct or indirect projections. This includes targets like the pretectum, hypothalamus and the superior colliculus which are important for pupillary reflexes, regulation of circadian rhythms and coordination of eye movements, respectively (Fernandez et al., 2016; Giolli et al., 2006; Scalia & Arango, 1979; Zhang & Hoffmann, 1993). The connections from retina to the

superior colliculus (SC) is termed a second visual pathway since SC is connected to many important areas involved in visual processing like the brainstem, LGN, V1 and the posterior parietal cortex. The posterior parietal cortex is part of the ventral stream and is important for spatial aspects of vison, including movement guidance, motion discrimination and visual attention. The importance of other visual pathways is demonstrated in a phenomenon termed "blind-sighted", where subjects who are blind after damage to visual cortex still have the ability to perceive light and moving objects. This is believed to due to the secondary visual pathway from retina via the SC (Barbur et al., 1993; Petruno et al., 2013; L. Wang et al., 2010).

Even though the posterior parietal cortex is thought of as close to an end-point in the dorsal visual stream after receiving carefully processed information from higher cortical sensory areas, it has been shown to be reciprocally connected to other areas as well. Thus, it might be more correct to think of visual processing as a continuous loop of feedback and feedforward information. For instance, the posterior parietal cortex (PPC) is connected to multiple thalamic nuclei including the lateral posterior nucleus (LP) and the lateral dorsal nucleus (LD) (Chandler et al., 1992; Conte et al., 2008; Kamishina et al., 2009) which in turn are connected to deeper layer neurons of V1 (Bortone et al., 2014; Bourassa & Deschênes, 1995; Deschênes et al., 1994; Zarrinpar & Callaway, 2006). Deeper layers of V1 are also directly connected to the SC and to the brainstem (Bourassa & Deschênes, 1995; Deschênes et al., 1994; Scanziani, 2016). All these connections suggest that V1 is not just a simple processing station for visual information on its way to higher cortical areas, but may be directly involved in modulating input before and after visual information reaches higher cortical areas. However, the functional roles of these interconnections remain elusive.

1.2 The primary visual cortex

1.2.1 V1 architecture and basic circuitry

The primary visual cortex is part of the neocortex and is organized into six distinct cell layers, labeled L1-L6, based on cell packing density, cell morphology and circuitry. The main recipient of sensory input from thalamus is L4. From here, the visual information is transmitted through cortico-cortical interaction in all layers and is then transferred to other cortical areas from the superficial cortical layers or to subcortical structures from the deeper

cortical layers. How each layer contributes to the information processing and how they interact has been a focus of investigation for more than 50 years, but is still not fully understood.

The basic feedforward signaling goes from L4 to L2/3, from L2/3 to L5 and higher cortical area, and lastly from L5 to subcortical areas including the SC and brainstem. In addition to this, local and distal axonal and dendritic arbors connect all layers together and it is believed that these recurrent intracortical connections serve to amplify and strengthen incoming signals (Han & Mrsic-Flogel, 2013; Lien & Scanziani, 2013; Reinhold et al., 2015). In fact, sensory input to L4 from the dLGN constitutes only 5-10 % of the synaptic input to neurons in L4 (Ahmed et al., 1994; Guillery & Sherman, 2002; Latawiec et al., 2000), illustrating that polyneuronal innervation from other cortical neurons is likely to play a significant role in visual processing. Sensory information from the retina arrives mainly in L4, but L6 also receive direct thalamic input from the dLGN (Briggs & Usrey, 2007; Constantinople & Bruno, 2013; Peters & Feldman, 1976). Recent findings indicate that the direct dLGN input to L6 serve a different function compared to the sensory information arriving in L4 (L. Wang et al., 2013), but what this function could be is still unknown.

Another important part of visual processing in V1 is feedback connections. This type of signaling is believed to be modulatory, and is supplementary to the primary visual input from dLGN. Higher cortical areas send feedback signals to L2/3 and L5 (Yang et al., 2013), and L5 sends strong feedback signals to L2/3 and weaker signals to L4 (Callaway, 1998). L6 is also very important when it comes to feedback as neurons here have direct projections back to the dLGN (Bourassa & Deschenes, 1995; Gilbert & Kelly, 1975; Thomson, 2010). Surprisingly, retinal afferents to the dLGN only constitute 5-10% of the synaptic input, where the remaining synapses are formed mostly by cortico-thalamic projections from L6 (Guillery & Sherman, 2002; Van Horn et al., 2000).

Neurons in the deeper cortical layers have been shown to exhibit several distinct functions and connectivity that suggest highly specialized functions. The L5 is intriguing as neurons here possess the only neocortical cell type that have dendritic trees spanning all six layers, as well as projections to subcortical area like the superior colliculus and the brainstem (Callaway, 1998; Gilbert & Kelly, 1975; Scanziani, 2016; Shai et al., 2015; Tsiola et al., 2003). The neurons in L6 have been subject to intense investigation the past decades because of their feedback connection to the dLGN. Several studies have revealed that L6 have a

modulatory effect on this primary thalamic nucleus, both directly and indirectly through the thalamic reticular nucleus (nRT) (Briggs & Usrey, 2007; Olsen et al., 2012; Thomson, 2010), suggesting that L6 can be part of regulating visual information even before it enters V1. Furthermore, L6 has been shown to have a modulatory effect in V1, both through excitatory connection as those to L5 (J. Kim et al., 2014), and also by recruiting local inhibitory networks to modulate activity across all layers (Bortone et al., 2014; C. C. Lee & Sherman, 2009; Olsen et al., 2012). The magnitude of cortical synaptic input that the dLGN receives, as well as the modulatory effect observed, suggest that these cortico-thalamic projections may be of great importance in visual processing. The input to L6 and the modulatory effect L6 show in V1 also raise some intriguing questions as to what its role in visual processing may be. However, the functional role and overall impact of the L6 feedback signaling and the cortical modulatory effects remain elusive.

1.2.2 Receptive fields from the retina to V1

Receptive fields in the visual system were first discovered in the retina of horseshoe crab by H. K. Hartline (1941) and soon after it was described in the mammalian retina as well (Kuffler, 1953). They observed that each retinal ganglion cell responds to stimulation of a central patch of photoreceptors, and that stimulation of the surrounding area resulted in the opposite response. This center-surround antagonistic organization of photoreceptors make up the ganglion cells' receptive field and based on their center-surround activation, ganglion cells can be classified into two classes; "on-center" and "off-center" cells. The receptive fields of the ganglion cells are overlapping and cover every part of the retinal surface, i.e. the entire visual field. This organization is maintained throughout the primary visual pathway in what is called retinotopic organization. This means that adjacent receptive fields of dLGN neurons, as well as V1 neurons, receive visual information from neighboring areas of the visual field.

While most receptive fields in dLGN have the same center-surround organization as retinal ganglion cells, receptive fields of V1 are different. Hubel and Wiesel (1959) were the first to demonstrate that cortical neurons in cat primary visual cortex respond to bars or edges, and only if the bars are presented at a particular angle (Figure 1.2). They discovered that neurons in the V1 are tuned to stimulus of specific orientation. Based on what stimuli the cells respond to, they can be further divided into simple cells with elongated receptive fields that detect edges of a specific angle or complex cells which are tuned to edges with a specific direction

of motion. Hubel and Wiesel (1974) also discovered that cells with similar orientation preferences are grouped into vertical columns, and that the orientation selective neurons horizontally adjacent to each other respond clockwise and counterclockwise with the full 180˚ cycle to their preferred orientations.

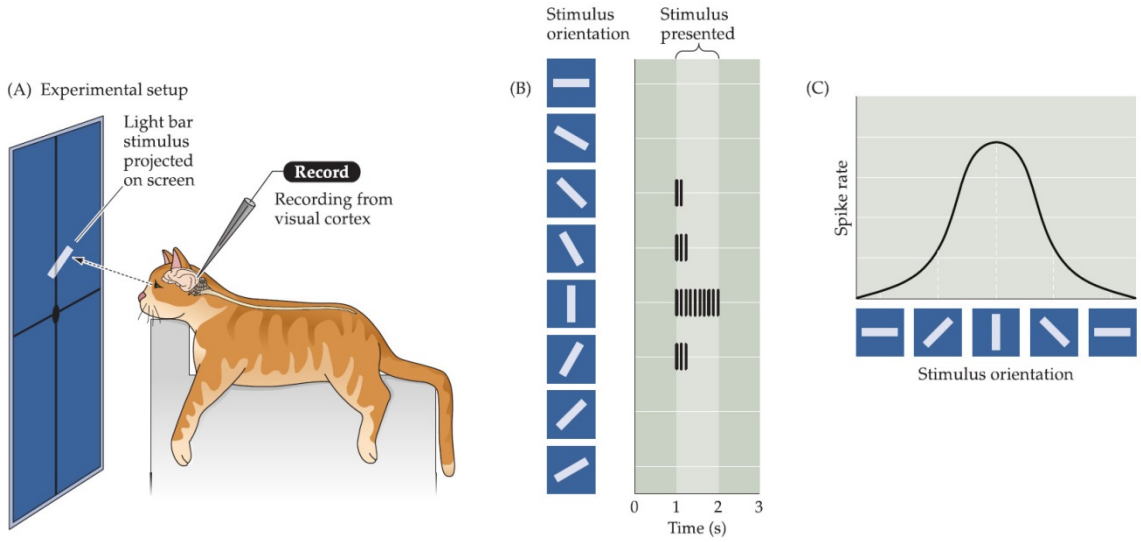

Figure 1.2: Hubel and Wiesel's original experimental setup demonstrating orientation selectivity in the primary visual cortex (V1). A) Moving light bar stimulus is presented to an anesthetized cat with a recording electrode in the V1 to record extracellular neuronal responses. B) Neurons in V1 respond selectively to bars or edges presented in particular angles illustrated by (C) the discharge rate in the tuning curve to vertical light bars at this particular orientation. The cells can also be direction selective, i.e. respond to light bars moving in a direction. For instance, if the vertical bar was moving to the left the neurons would be selective for light bars at 180˚ or moving to the right to 0˚ (Figure 12.8, Purves et al., 2012).

The dLGN is generally thought of just as a relay station for visual processing, and textbooks describe them to have only circular center-surround receptive fields which combine to give orientation and direction selectivity in the cortex. However, recent studies in mice suggest that some dLGN neurons also have orientation selectivity (Marshel et al., 2012; Niell, 2013; Piscopo et al., 2013; Scholl et al., 2013; Zhao et al., 2013). It is speculated that this orientation selectivity in dLGN arise from direction selective retinal ganglion cells (Cruz-Martin et al., 2014; Huberman et al., 2009; Piscopo et al., 2013; Scholl et al., 2013), and that it is not due to cortical feedback (Scholl et al., 2013; Zhao et al., 2013). However, the function of these orientation selective dLGN cells neurons, as well as their targets, is yet to be identified.

It is still not fully understood how orientation selectivity in cortical neurons arise. The simplest model is the original feed-forward model of Hubel and Wiesel (1962). They proposed a model consisting of two processing stages: firstly, the summation of input from dLGN neurons whose receptive fields are arranged in rows and secondly, the filtering of summed inputs by a spike threshold, which can be altered by cortical intervention. The first processing stage implies that the dLGN input serve as the origin of orientation tuning, while intracortical circuits serves to amplify and strengthen the incoming signal. This has been confirmed in multiple studies (Chung & Ferster, 1998; Han & Mrsic-Flogel, 2013; Li et al., 2013; Lien & Scanziani, 2013; Reinhold et al., 2015; Shapley et al., 2003). The second processing stage, involving a spike threshold, is added so that random dLGN activity will not give rise to undesired firing of action potentials in orientation-tuned cells. Action potentials are all-or-nothing responses; stimuli below threshold will not produce a response, but summation of stimuli above threshold produce signals of same amplitude. This gives room for the idea that inhibitory neurons could be involved in shaping the orientation selectivity of cortical neurons through inhibitory input that ultimately affect the summation of signals to a spike threshold. Inhibition by interneurons has been shown to sharpen the orientation tuning of the cortical cells and affect the amplitude of the signals (Crook et al., 1998; S. Lee et al., 2012; Liu et al., 2011; Shapley et al., 2003). The role of different inhibitory neurons in this process is not fully understood, and is yet to be established.

1.2.3 Visual processing in rodents

The primary visual pathway of rodents and other mammals share common features but are also different in regards to architectural and functional organization. One difference is the positioning of the eyes that are laterally positioned in rodents, whereas higher mammals, such as cats and primates, have frontal eye positioning (Figure 1.3). Consequently, the visual system in rodents is mostly devoted to monocular vision since there is little overlapping of the visual field (the binocular zone) of the two eyes (Priebe & McGee, 2014; Wallace et al., 2013). This is demonstrated by the fact that almost half of the retinal ganglion cell axons crosses over in the optic chiasm in primates, whereas 4 % of the retinal ganglion cell axons cross to the ipsilateral hemisphere in rodents (Priebe & McGee, 2014). Furthermore, the LGN is organized differently in rodents. While higher species have six cell layers in the LGN, which all receives input from the retina, the LGN of rodents is divided into three subdivisions (DeFelipe, 2011). These subdivisions are the dorsal and ventral lateral geniculate nucleus

(dLGN and vLGN) and the intergeniculate leaflet (IGL) (Harrington, 1997; Priebe & McGee, 2014). It is the dLGN that receives most of the retinal input, as well as modulatory input from different areas of the brain. While higher order species have columnar organization as explained in previous sections, this columnar organization is not found in rodents. Even though rodents do not display complex organization in dLGN and V1, rodents too possess simple and complex cells that have highly selective receptive fields in the primary visual cortex (Niell & Stryker, 2008) as well as retinotopic organization (Gias et al., 2005; Q. Wang & Burkhalter, 2007). However, a more simple visual system makes rodents good candidates for studies of early visual processing particularly for the opportunities for genetic manipulations.

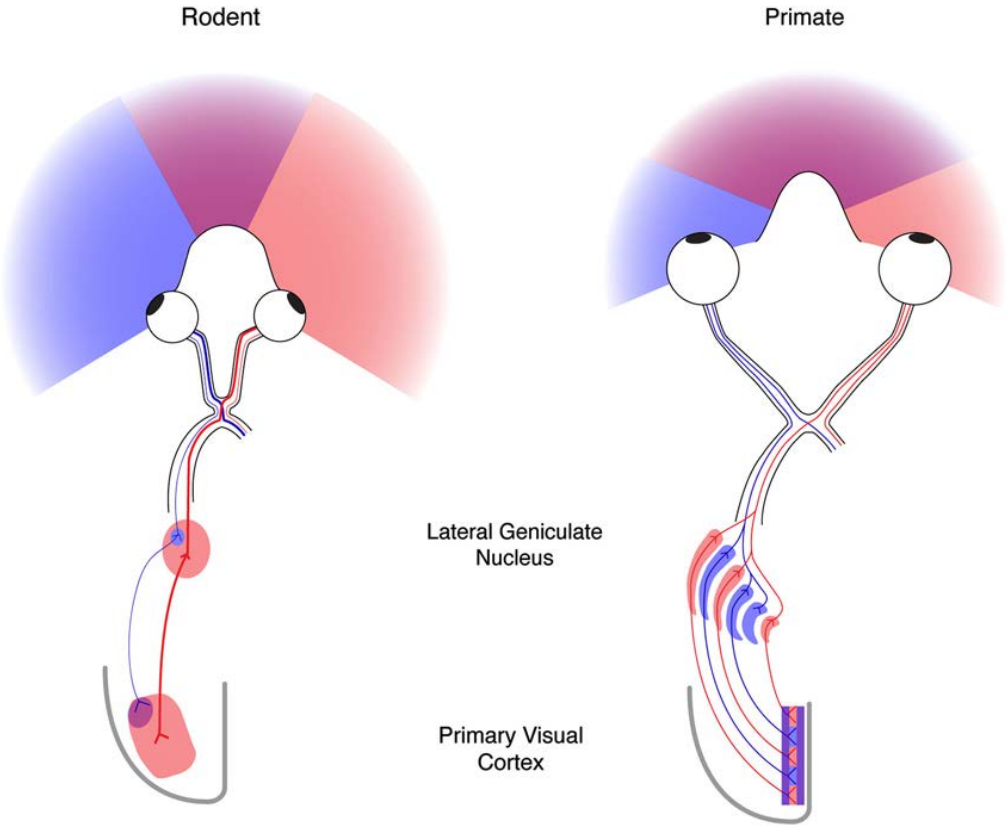

Figure 1.3: Differences between rodent and primate visual system. The eyes are positioned laterally in rodents, whereas primates have frontal eye location, resulting in less overlapping of each eye's visual field (binocular zone) in rodents, and their visual system is more devoted to monocular vision. Furthermore, the LGN in rodents is not highly organized as seen in animals with better visual acuity like cats and primates. Lastly, the primary visual cortex in rodents do not have columnar organization, however V1 neurons do have highly selective fields, as well as retinotopic organization. Figure from Priebe & McGee (2014).

1.2.4 Non-geniculate impact on orientation selectivity

From the section above it is established that the origin of input to create the receptive fields of V1 neurons comes from dLGN, but non-geniculate input also affect the visual response. There is strong interest for understanding how specific neuron population, behavioral states, or cortical and subcortical areas influence receptive field properties.

As explained, L6 has received particular attention due to the intriguing reciprocal connectivity between L6 and the dLGN. Receptive field structures vary from layer to layer within V1 (Grieve & Sillito, 1991a; T. Kim & Freeman, 2016; Martinez et al., 2005; Velez-Fort et al., 2014), and there have been controversies regarding whether L6 influences receptive field properties of upper layers (Allison et al., 1995; Bolz & Gilbert, 1986; Grieve & Sillito, 1991b). Despite these controversies, it is becoming clear, through both chemical and optogenetic perturbations of L6, that L6 play a crucial role in regulating gain in orientation selective neurons in V1 as well as the dLGN, and that the overall impact is suppressive (Bortone et al., 2014; Grieve & Sillito, 1991a; Olsen et al., 2012). It still not known what inputs drive and modulate the activity of L6 or why they seem so highly specialized.

Other sensory information not directly related to the primary visual stream, like movement and behavioral states, also play a part in visual processing. Until recently, the majority of studies on the visual system were conducted in anesthetized animals, which excludes the effect of behavior on visual processing. In the few studies performed in awake animals it has been shown that neuronal activity is higher in awake animals (Fontanini & Katz, 2008; Greenberg et al., 2008; Livingstone et al., 1996) and that locomotion increase the responses in V1 without changing the orientation selectivity (Keller et al., 2012; Niell & Stryker, 2010). Furthermore, it has been shown that responses in L2/3 of mouse V1 are strongly driven by locomotion and by mismatch between actual and expected visual feedback (Keller et al., 2012). It has been suggested that the enhanced visual response by movement could be due to vasointestinal peptide (VIP) positive inhibitory neurons that are activated during movement (Fu et al., 2014). Optogenetic activation of these neurons in stationary awake animals mimicked the effect of locomotion on excitatory neurons in V1. It has also been demonstrated that attention enforces a significant effect on the visual response (Bereshpolova et al., 2011; Reynolds & Heeger, 2009; X. Wang et al., 2014) and that alertness could lead to sharper orientation selectivity (Zhuang, 2014).

The studies mentioned above are all conducted in head-fixed animals, excluding the effect of head movement and vestibular inputs to orientation selectivity. However, studies in anesthetized cats and alert monkey show that head tilt do affect visual processing (Denney & Adorjanti, 1972; Sauvan, 1999). The responses of neurons in V1 in these experiments were variable; while most neurons lost selectivity or shifted orientation during head tilt, other neurons were of compensatory nature, preferring the same orientations regardless of head rotation. As head tilting naturally occurs during movement, these results confirm an important principle of visual processing; the visual scene is not stationary - the body moves around, the eyes moves and the visual scene move. How movement impacts visual information processing remains not fully understood.

The findings mentioned in this section suggest that body position, movement and behavioral states all integrate in the early processing, but it is still little research to demonstrate how orientation selectivity in V1 is affected with all systems in action. Studies with freely moving animals has led to remarkable discoveries in other brain areas such as hippocampal place-cells (O'Keefe & Dostrovsky, 1971), head-direction cells (Taube et al., 1990), and grid cells in the entorhinal cortex (Fyhn et al., 2004; Hafting et al., 2005). These findings clearly demonstrate the importance of the animals' interaction with the environment to be as natural as possible to fully understand how a neuronal system in the brain works. Thus, in the current project I wanted to study the visual processing in animals free to move around. Recent preliminary experiments from our research group indicate that a small subpopulation of neurons recorded from the deeper layers of V1 in freely behaving rats displays orientation tuning which is resistant to the animal's head and body movements (I.E.J. Aasebø, unpublished). The remarkable activity patterns of these initial findings may be highly important for our understanding of visual information processing and the cortico-thalamic recurrent network. However, the functional properties of these cells, their relation to neighboring neurons, their distribution in the visual cortex or role for information processing remain elusive and will be the focus of my study.

1.3 Aims of the study

The objective of this study was to investigate the effect of movement on orientation selective neurons in the primary visual cortex by recording from single units in awake, freely moving rats. This was achieved by:

- recording single unit activity from deep layers of the visual cortex during visual stimulation across different behavioral conditions.
- examining the effects of movement on the orientation selectivity of single units recorded.
- examining orientation selectivity of single units at different locations in the primary visual cortex.
- investigating reciprocal connections from layer 6 of the primary visual cortex to thalamic nuclei by use of neuronal tracers.

2 Materials and methods

2.1 Approvals and research animals

The experiments were approved by the Norwegian Animal Research Committee (FDU) prior to initiation and all the practical work was carried out at the Department of Biosciences, Faculty of Mathematics and Natural Sciences, the University of Oslo. Participating parties have completed a course in Experimental Animal Research and are all approved by the FDU. The animal facility and experiments using animals are in accordance with the Norwegian Animal Welfare Act and the European Convention for the Protection of Vertebrate Animals used for Experimental and Other Scientific Purposes.

The experiments were conducted with locally bred Long Evans hooded rats. All animals weighed 400-500 g, and were between 3-6 months old. Animals were kept on a 12h light/dark cycle with lights on from 20:00 to 08.00. All the recordings were performed in the dark phase since rodents are nocturnal animals and are active during the dark phase. Prior to any experiments the animals were housed in groups of three to four in polycarbonate cages (35x55x19 cm) from Scanbur A/S with woodchip bedding and plastic toys. Food and water were available ad libitum. After surgery the animals were housed separately in transparent plexiglass cages (35x55x30 cm) to minimize the risk of injury to the animal and the microdrives mounted on their heads. To maintain body weight during the experimental period the animals were given 6-8 food pellets daily in addition to ad libitum access to water. The ventilation rate in the housing facility is maintained at 5-20 times per hour, the humidity at 55 ± 10 % and the temperature is kept at approximately 21˚C. The light intensity in the light phase was more than 100 lux.

2.2 Surgery Preparations

2.2.1 Tetrode and Microdrive assembly

The tetrodes were created by first making a loop from a single thread of 17 µm-diameter platinum-iridium wire (California Fine Wire Company, CA, USA) with a small piece of tape. The wire was then twisted around a metal arm above a magnetic stirrer to create two loops.

To intertwine the four threads of wire making up the loops, a hook with a magnet was hung at the bottom, and when the magnetic stirrer was switched on the wires twisted around each other making a tetrode. The intertwined wires were then heated for the heavy polyimide enamel insulation to fuse for 25 seconds by a heat gun to obtain a more robust structure. The tetrode was then cut free giving one end with intertwined wires and one end with four free ends. To complete the tetrode, the insulation was removed at the tips of the four free ends by burning them with a lighter for half a second.

Four of these tetrodes were then assembled onto a microdrive (Axona Ltd, Herts, UK) by twisting the free electrode ends around conductive cables on the microdrive. Hence, the microdrive carries sixteen electrodes upon completion. To ensure optimal electric connection between the electrodes and the wires of the microdrive, they were secured with conductive silver paint (HK Wentworth, Leicestershire, UK) and layers of nail polish. In order to obtain optimal resistance of the wires and thus increase the sensitivity of the electrodes, the impedance of each electrode in the intertwined end was lowered from around 1200 kΩ to 140-220 kΩ by electroplating them in platinum solution (Ferguson et al., 2009).

2.2.2 Injection preparations

Glass pipettes for injections were pulled from capillary glass tubes with an outer diameter of 1.2 mm, using a P-30 micropipette puller (Sutter Instrument Company, CA, USA). The finished pipette had a taper length of 5-10 mm and an opening diameter of 15-20 µm. The retrograde tracer Cholera Toxin subunit B (CTxB) conjugated to AlexaFluor 594 (Life Technologies, CA, USA) was reconstituted in filtered phosphate-buffered saline (PBS) to a final concentration of 1 µg/µL. A viral vector carrying Channelrhodopsin 2 (ChR2) and a green fluorescent protein tag (AVV5-Syn-ChR2-GFP, Penn Vector Core, PA, USA) was used for anterograde tracing. Both tracers were stored in smaller aliquots at -80º which were thawed on ice immediately before use.

2.3 Surgical procedures

All surgeries were performed in collaboration with PhD students Ida E. J. Aasebø or Kristian K. Lensjø. They assisted in lowering and securing the tetrodes and with the microinjections.

Prior to every surgery, equipment was heat sterilized at 150˚C for 90 minutes and cotton swabs autoclaved. The work area and the stereotaxic frame were disinfected with 70 % ethanol in order to minimize the risk of infection. All animals were initially placed in an induction chamber with 5 % isoflurane (Baxter, Oslo, Norway). Animals were then either placed in a mask with isoflurane mixed with air at a constant flow of 2 L/min which was gradually lowered during the surgery to 1.5-2 %, or given an intraperitoneal injection of a Ketamine/Medetomidine (Ketamine 75 mg/kg, Medetomidine 0.75 mg/kg) mixture. In case of the latter, additional small injections were made if required during the course of the surgery. The hind paw withdrawal reflex was used to determine the depth of anesthesia before and during surgery.

After anesthesia was induced, the animals were head fixed in a stereotaxic frame (World Precision Instruments Ltd, Hertfordshire, UK) by placing ear bars into the external auditory canal and by using the height-adjustable nose-clamp to obtain a planar skull position. The midline of the skull should then be aligned with the frame, allowing stereotaxic measurements of coordinates. After head fixation, the animals' head was shaved from between the eyes to roughly between the ears followed by disinfection of the area with 70 % ethanol and a chlorhexidine and iodine solution (2 %). The animals were then given subcutaneous (s.c.) injections of Temgesic (buprenorphine, 0.04 mg/kg) and local s.c. injections of Marcain adrenalin (bupivacaine; adrenalin, 1 mg/kg) prior to any incisions. Throughout the surgery the breathing rate, blood O_2 saturation, heart rate and core temperature were continuously monitored by a MouseStat system (Kent Scientific, CT, USA).

The first incision was a longitudinal cut in the skin with a scalpel. Skin, muscle tissue and membranes were then moved and held aside by artery clamps to expose the underlying skull. To prevent the skull and surrounding tissue from drying out and also to prevent heat damage during drilling, sterile 0.9 % NaCl solution was applied throughout the procedure. The intersection of the sagittal and lambdoidal skull sutures, lambda, was used as a skull landmark to measure out the bilateral coordinates for the craniectomies. The coordinates for V1 was in accordance with the atlas of the rat brain by Watson and Paxinos (2007). The craniectomies were created using a hand-held dental drill (Perfecta-300, W & H Nordic, Täby, Sweden). For the microdrive surgeries, additional holes were made for grounding and stabilization of the implants by using a dental drill mounted to the stereotaxic frame. Three jeweler's screws were embedded in the skull posterior to lambda and four screws embedded anterior to bregma, the

latter included two screws that served as ground reference for the tetrodes, resting on the surface of the brain with ground cables soldered to the screw (Figure 2.1).

Towards the end surgical procedures, animals were given an s.c. injection of Rimadyl (carprofen 5 mg/kg). Post-operative care included cleaning with 70 % ethanol and application of an antibiotic ointment (Fucidin, Leo Pharma, Oslo, Norway) on the edge of the wound if necessary, and s.c. injections of Rimadyl (carprofen 5 mg/kg) daily for three days to relieve postoperative pain and reduce inflammation.

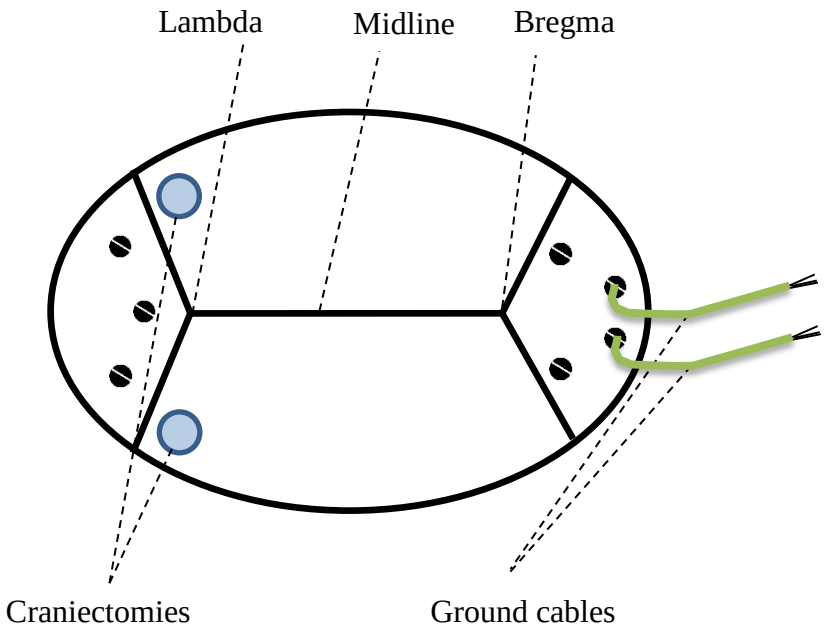

Figure 2.1: Sketch of the skull landmarks, craniectomies and screw holes. Seven screws were embedded in the exposed skull for stabilization and grounding. Four of the crews were anterior to bregma, including two with ground cables, and three posterior to lambda. Bilateral craniectomies were used for injection of tracers and for insertion of tetrodes.

2.3.1 Microdrive implants

The mediolateral and anterioposterior coordinates and the angle of the tetrodes varied between animals in order to find the optimal location of the units we were aiming for in V1. Also, the final position of the tetrodes was adjusted to avoid visible blood vessels in the cortex when lowering the tetrodes. The dorsoventral coordinates were adjusted to also obtain electrophysiological recordings from more superficial layers in some of the animals.

Postmortem histological inspection of the tetrode tracks revealed that most implants were within the monocular region of V1 or on the border between the binocular and monocular regions. The following coordinates were used for microdrive insertion: AP: 2.5±0.5 mm anterior to the transverse sinus, ML: 4.5±0.5 mm, DV: 0.7±0.2 mm, Angle: 0-30º (AP: anterioposterior, ML=mediolateral, DV=dorsoventral).

The microdrives were mounted onto holders attached to stereotaxic towers on the frame. A small incision was made in the dura to allow the tetrodes to easily penetrate the cortex and be lowered into position. Surrounding the tetrodes was an outer cannula which was slid down on the dura for protection of the tetrodes. The craniectomies were then covered with Spongostan (Ethicon, Norderstedt, Germany) to protect the brain from dental acrylic cement (KA Rasmussen, Oslo, Norway) which is used to secure and stabilize the microdrives by attaching to the implant itself and the screws embedded in the skull. Lastly, the ground cables of the microdrive were soldered onto the ground cables attached to the foremost screws. Fucidin was then applied to the edge of the wound to prevent bacterial growth. The total weight of the microdrive implant taken together with the dental cement was approximately 7 grams, constituting 1.5-1.75 % of the body weight of adult rats (400-500 g). The tetrodes were lowered deeper into the cortex by a turning mechanism on the microdrive in steps of 50 µm.

2.3.2 Microinjections

For the microinjections two different tracers were used. One of the tracers was an anterograde viral vector carrying Channelrhodopsin 2 and a green fluorescent protein tag (AAV5-syn-ChR2-GFP, Penn Vector Core, PA, USA) which was injected into the deeper layers of V1. The second tracer was the retrograde Cholera Toxin subunit B (CTxB) conjugated to AlexaFluor 594 (Life Technologies, CA, USA) which was injected into the dLGN.

Coordinates for the microinjections were:

AAV5-syn-ChR2-GFP:	AP: lambda	ML: 3.9 mm	DV: 1.2 mm
CTxB:	AP: bregma-4.8 mm	ML: 3.8 mm	DV: 4.2 mm

The microinjections were conducted with a NanoJect II (Drummond Scientific Company, PA, USA) which was mounted to the stereotaxic frame. The glass pipettes used had a taper of 5 mm, and a tip with a 15-20 µm opening. They were backfilled with mineral oil before use and

then assembled into the micro injector and loaded with the tracer. In each location we injected 200 nL in a step-wise manner over a period of 10-15 minutes. The pipette was left in the tissue for 10 minutes after injections to allow for the tracer to diffuse into the tissue.

Following the injections, KWIK-SIL silicone (World Precision Instruments Ltd, Hertfordshire, UK) was used to fill the craniectomies. The incision was then closed with sutures and the edge of the wound was coated with a thin layer of anti-bacterial Fucidin ointment.

2.4 Electrophysiological recordings

2.4.1 Recording setup

The animal was allowed to recover from surgery for a minimum of three days before the first electrophysiological recordings. Prior to the surgery the animals would be handled, and this eased connection of the microdrive to the recording equipment after surgery, as the rat would be used to human touch and scent. The connected animal was then placed in a glass box (25x25x35 cm), enclosed by four 17” computer monitors (Dell Computers, Limerick, Ireland) where visual stimulation in the form of drifting gratings were presented during recordings.

The recordings were conducted and neuronal activity was compared during two conditions; movement and sessile behavior. The movement recordings were conducted when the animal was moving around and exploring in the box. Small bits of chocolate treats, or introduction to new scents, were sometimes used to get the animal to explore the box. In order to obtain recordings during sessile behavior, with minimal movement of the animal’s head, the animals were left to explore the box and its surroundings for 5-15 minutes after which the animals usually laid down, and the recording started. The animals’ behavior was monitored by over-head tracking, and the recording stopped if the animals started to move. Spike sorting was conducted after each trial, and if there were no units with apparent orientation tuning in response to visual stimulation, the tetrodes were lowered 50 µm (up to 200 µm per day).

The microdrives were connected to a multichannel head stage which was coupled to a lightweight cable and a pre-amplifier which was connected to the 32- or 64-channel recording unit (Axona, UK). To allow the animal to move freely inside the box, a counter-weight system was installed to relieve the extra weight of the cables and head-stage. The Axona

recording software also provide a digital amplifier, hence, both digital and analogue amplifiers were used in all the experiments. A threshold was set and data was collected when the signal amplitude exceeded at least two to three times the noise level. All signals were band-pass filtered between 0.8 and 6.7 kHz and were amplified 8 000-15 000 times. Triggered spikes were stored at 48 kHz (50 samples/waveform, 8 bits/sample) with a 32-bit time stamp (clock rate 96 kHz). Spike waveforms reaching a threshold of 50-80 µV were time-stamped and digitized at 32 kHz for 1 ms, and were stored to the hard-drive for offline analysis. Out of the total 32 channels used for recording, two of them were used to record the local field potentials (LFP) from each hemisphere. The LFP signal was amplified 2000 times, lowpass-filtered at 500 Hz and stored at 4.8 kHz (16 bits/sample). Synchronized time-stamping of stimuli and spikes were achieved through a connection between the computer used to generate the visual stimuli and the computer for electrophysiological recordings.

The rat's position and movement was monitored by using the dacqUSB tracking system. Two infrared light-emitting diodes (LEDs) were attached to the head stage of the animal and the LEDs position was tracked at a rate of 50 Hz. The boundaries for tracking were defined in the software before recording, covering only the glass box and not the surroundings. The movement was later analyzed as described in section 2.6.1.

2.4.2 Visual stimulation

In order to detect orientation selective units, the animals were presented with visual stimulation in the form of drifting gratings or bars. A stimulus regime of drifting gratings with 8 different orientations repeated 12 times were used to identify visually evoked units (Figure 2.2). Each orientation would be presented in random order for 0.5 seconds, followed by 0.3 seconds of a gray screen. In order to optimize the responses, the spatial frequency was set to 0.08 cycles per degree of visual angle, and the temporal frequency to 4 Hz (Girman et al., 1999; Niell & Stryker, 2010). The sessions were recorded when the animal had as little movement as possible to avoid high noise levels due the animal scratching or cleaning itself, as well as self-motion. All units that were easily separable in the preliminary spike sorting conducted shortly after recording were checked for orientation selectivity using custom Matlab software (data analysis section 2.6). Due to time constraints for analyzing data, units that were difficult to separate were excluded from further analyses.

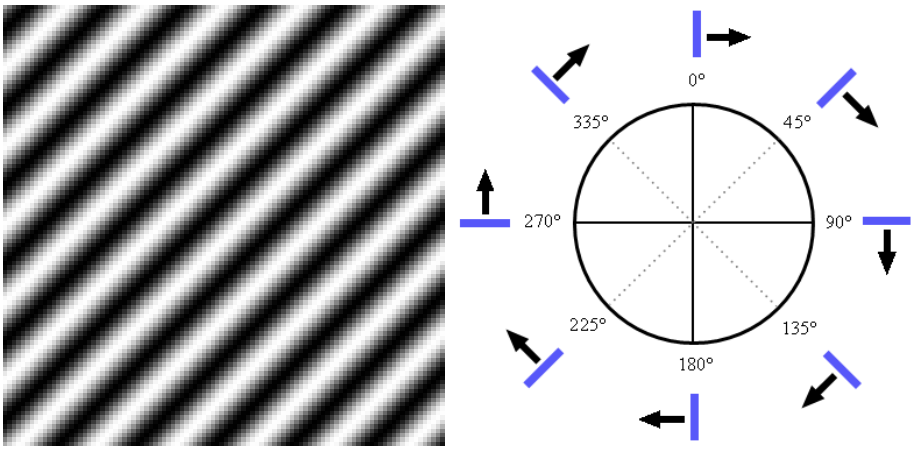

Figure 2.2: Drifting gratings were presented as visual stimuli to identify visually modulated neurons. Stimulation was presented randomly in 8 or 16 different orientations for half a second each in 12 repetitions.

When a unit showed orientation selectivity, additional sessile recordings and movement recordings were conducted in order to investigate if orientation selectivity remained stable across consecutive sessions and between sessile and movement behaviors. For each session with visual stimulation a time-stamped log file was generated and stored which allowed for stimulus-response analysis.

If orientation selective units were located, the following recording session were conducted:

1. Four sessile recordings where the animal showed little or no movement.
   2 x drifting gratings; 8-16 orientations in random order; 12 repetitions

2. Four movement recordings that included periods of movement.
   2 x drifting gratings; 8-16 orientations in random order; 12 repetitions

3. Two sessile recordings using orientations spanning 180˚ over the preferred direction; for instance 0-180˚ if the units preferred orientation is 90˚.
   2 x drifting gratings; 36 orientations in random order; 12 repetitions

4. Two movement recordings using orientations spanning 180˚ over the preferred direction; for instance 0-180˚ if the units preferred orientation is 90˚.
   2 x drifting gratings; 36 orientations in random order, 12 repetitions

2.5 Histology

2.5.1 Perfusion

To verify the recording location of the tetrodes, and for immunohistochemical investigations, animals were sacrificed shortly after the last electrophysiological recordings and transcardially perfused to fixate the brain. The perfusion procedure was the same used for animals injected with tracers.

Animals were given an intraperitoneal overdose of pentobarbital sodium (50 mg/kg). When deeply anaesthetized and having no response to pinching of the hind-leg, animals were transcardially perfused with 0.9 % NaCl solution, followed by 4 % paraformaldehyde (PFA) in PBS. The brains were dissected out and left to post-fixate in 4 % PFA overnight before being transferred to a 30 % sucrose solution in PBS for three days at 4˚C. Sucrose is a cryoprotectant which dehydrates the tissue, and prevents formation of ice crystal artefacts. The brain was then flash-frozen with CO2 freezing spray and cut into coronal sections of 40 µm using a cryostat (Ortomedic, Lysaker, Norway). The sections were either collected directly on Superfrost plus glass slides (Thermo Fisher Scientific, Oslo, Norway), or transferred into PBS for immunohistochemistry staining.

2.5.2 Nissl staining

Sections with tetrode tracks were stained for cell bodies using Nissl staining, which selectively targets extranuclear granules of RNA in the so-called Nissl bodies found only in neurons. The dried sections were gradually hydrated in 100 %, 90 %, 80 %, 70 % ethanol and dH_2O, respectively, and immersed in Cresyl Violet staining solution. After staining the sections were dehydrated again using 70 %, 80 %, 90 %, 96 % + acetic acid, 100 % ethanol and xylene, respectively, and secured with a cover slip using Entellan (Merck Millipore, Darmstadt, Germany). The sections were investigated, measured and photographed under a microscope. When assessing the tetrode depth, an estimated shrinkage of the tissue of up to15 % was taken into account (M.P. Witter, personal communication)

2.5.3 Immunohistochemistry staining

Immunohistochemistry was used to visualize the tracer injections and labeled projections. Detailed protocols are described in appendix 6.3. All procedures with antibodies were conducted on free-floating sections to allow for maximal antibody penetration of the tissue. Sections were rinsed in PBS and then blocked with 1 % bovine serum albumin (BSA, Sigma-Aldrich, Darmstadt, Germany), 0.03 % Triton x-100 (Sigma-Aldrich, Darmstadt, Germany) in PBS for one hour to reduce nonspecific antibody reactivity. Sections were then incubated in block solution with the primary antibody overnight at room temperature. The following day sections were rinsed in PBS and incubated with the secondary antibody in PBS for two hours. After incubation, sections were rinsed in PBS, mounted on Superfrost Plus glass slides (Thermo Fisher Scientific, Oslo, Norway) and left to dry. Lastly, the sections were rinsed in dH_2O to remove excess salt from the PBS, and then secured using Fluorsave Reagent (Calbiochem, Merck Millipore, Gemany). The primary antibodies used were rabbit anti-GFP (A11122, Life Technologies, CA, USA, used in a 1:1000 dilution) and rabbit anti-PCP4 (HPA005792, Sigma-Aldrich, Darmstadt, Germany, used in a 1:400 dilution). The secondary antibody used for both staining procedures were goat anti-rabbit Alexa 488 (A11034, Life Technologies, CA, USA, used in equal dilutions as previously used primary antibody).

The sections from the animal injected in V1 with anterograde AAV5-Syn-ChR2-GFP, were sampled from 3.3 mm to 5.3 mm anteriolateral from bregma to include the entire dLGN. There were also some sections from the injection site in V1. The antibodies used, fluorescently label the GFP tag in the ChR2-GFP protein expressed in the cell membrane of infected axonal projection terminals from V1.

The CTxB tracer was injected in the dLGN in order to retrogradely label the feedback projection from L6 to dLGN. For this reason, the sections were sampled from V1, 5.8 mm to 7.8 mm anteriolateral from bregma, and also some sections from the injection site. The antibodies used recognizes Purkinje cell protein 4 (PCP4), which is a marker for excitatory neuron subtypes in deeper layers of the visual cortex (Watakabe et al., 2012).

Additionally, some sections were stained with PCP4 and counterstained with fluorescent Nissl to ease the identification of the cell layers. The PCP4 staining was performed as described above and sections were then transferred to a 1:100 NeuroTrace Fluorescent Nissl stain diluted in PBS and incubated for 30 minutes. After incubation, the sections were washed in a

0.1 % Triton X-100 in PBS solution and incubated at room temperature for 10 minutes. Following this incubation, the sections were washed in PBS and mounted on Superfrost plus glass slides and left to dry. Lastly, sections were washed with ddH_2O to remove excess salt from the PBS and then covered with a coverslip using FluorSave Reagent.

All sections were photographed using an Axiocam HRZ camera (Carl Zeiss, Oberkochen, Germany) through an Axioplan 2 microscope (Carl Zeiss, Oberkochen, Germany). The MosaiX module in the AxioVision software was used to stitch together the high-resolution images. Images were edited using Adobe Photoshop CS6 (Adobe, CA, USA).

2.6 Data analysis

2.6.1 Analysis of behavioral condition

Preliminary behavior analysis was performed using Tint (Axona Ltd, Herts, UK) which gives the rat's trajectory and heat map of activity. Additional movement analyses of the sessions were performed using the program AnalyseWM (Axona Ltd, Herts, UK). The .pos-files were used as input to generate trajectory plots and occupancy maps, as well as to perform segment analysis, find path lengths and other general measures.

2.6.2 Spike sorting and waveform analysis

The graphical cluster-cutting software Tint (Axona Ltd, Herts, UK) was used for manual spike sorting. The software use two-dimensional scatter plots based on waveform amplitude of single action potentials from each of the electrodes. Spikes from the same unit tend to form distinct clusters that separate from the noise and from spikes from other units (Figure 2.3). To ensure that noise was removed from unit activity, each cluster was enclosed with a boundary which was verified by performing cross-correlation analysis; if the lag period between spikes within a cluster was shorter than 1 ms, the cluster was presumed to contain spikes from more than one unit or noise and would be separated accordingly. As mentioned previously, units that didn't separate easily during spike sorting were left out from further analysis due to time constraints of the thesis.

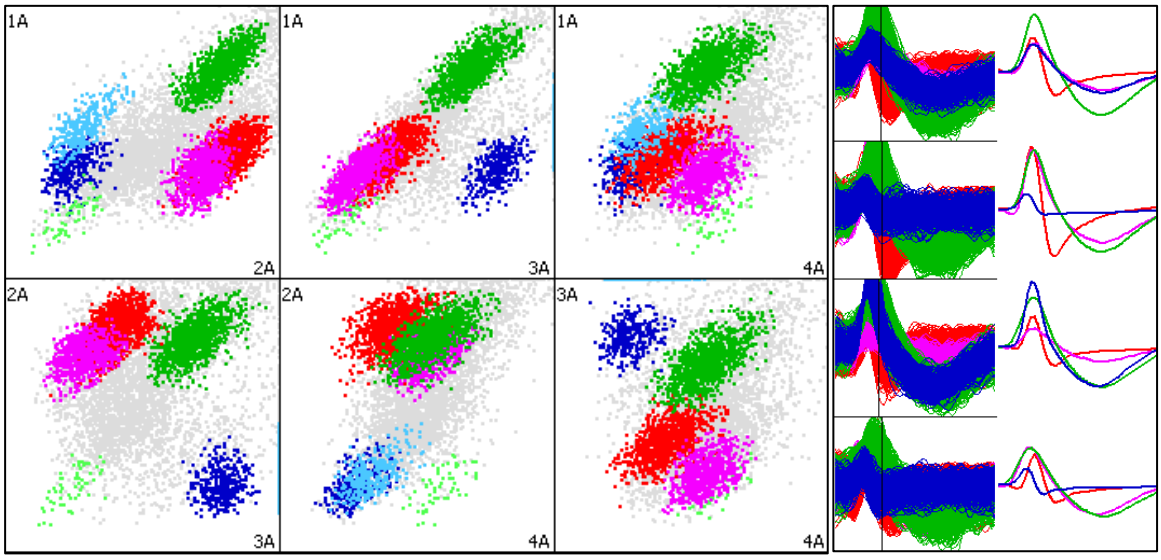

Figure 2.3: Spike sorting in the cluster-cutting software Tint. Single spikes' amplitude is plotted for each electrode (1A-4A) in scatter plots shown to the left (absolute values for µV not shown). Spikes from the same units are registered differently on all electrodes and cluster into clouds of spikes that can be separated (color-coded) from the noise (gray) and spikes from other units. Right panel: waveform and mean waveform of four clusters separated in the cluster cutting procedure.

Using the Matlab program AxWaveform 2.1 (R. Skjerpeng, Norwegian University of Science and Technology and T. Hafting, University of Oslo), units were classified as either putative inhibitory or putative excitatory pyramidal cells. The .cut-files generated by Tint was used, and unit classification was made based on the average waveform from the electrode with the highest amplitude, including duration in time from wave peak to wave trough, wave peak to baseline and wave amplitude (Bartho et al., 2004; Bruno & Simons, 2002; Niell & Stryker, 2008). Output values from the program were exported to Microsoft Excel, and units were separated into putative excitatory and inhibitory neurons comparing the half width of the amplitude and the peak to trough duration (Figure 2.4).

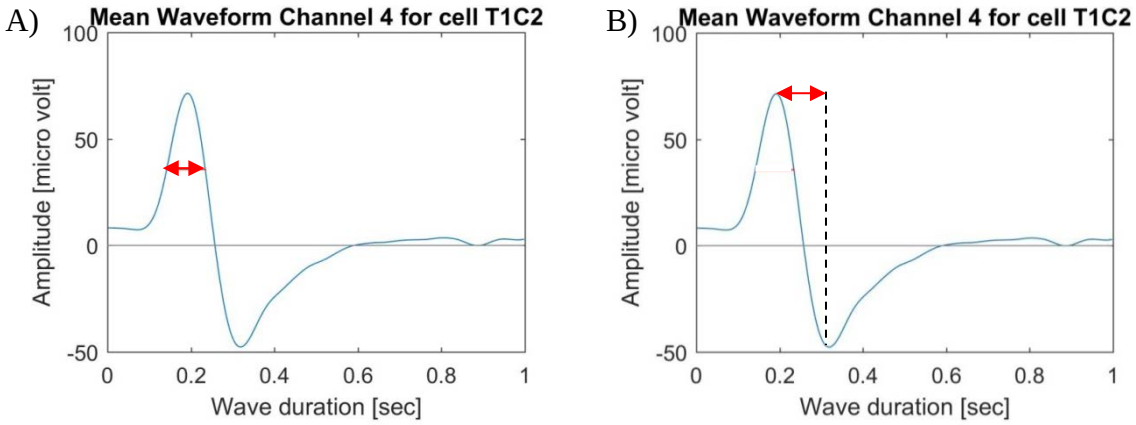

Figure 2.4: Classification of unit activity into putative inhibitory or excitatory units. Units were separated based on comparison between the peak to trough time (A) and the half width of the amplitude (B) (red arrows).

2.6.3 Orientation tuning analysis

The orientation selectivity of the units was determined using custom Matlab software which correlates the time-stamped log files from the visual stimuli to the time-stamped cluster files of sorted spikes. The tuning curve of the unit was generated as a relationship between the average firing rates distributed over the different orientations presented during visual stimulation. A raster plot with the occurrence of spikes in the given cluster in response to the orientations presented during visual stimulation was also generated. An orientation selectivity index (OSI) was calculated using the ratio $(R_{pref} - R_{orth}) / (R_{pref} + R_{orth})$ where R_{ort} was the mean firing rate response of the two directions orthogonal to the preferred orientation (Allen Brain Observatory, 2016; Zhao et al., 2013)

2.6.4 Statistical analysis

All statistical analyses were performed using Prism 6 (Graphpad). Shapiro-Wilk test was used as a test for normality, and Levene's test was used to assess equal variances. If the data was normally distributed and showed variance homogeneity, paired t-tests were used within groups, and one-way ANOVA with a Tukey's multiple comparisons test was used across groups. If the data had uneven distribution or failed the equal variances test, Wilcoxon signed-rank test was used within groups, and Kruskall-Wallis test with a Dunn's multiple comparisons test was used between groups.

3 Results

In this project, a total of 12 male Long Evans rats were used. Of these, ten were used for electrophysiological recordings and two for tracer injections. In addition, data and histology from two other animals (surgery and experiments conducted by PhD student Ida E.J Aasebø) were also included in the analyses. A total of approximately 800 neurons were recorded from these animals. When screening for orientation-tuned neurons, preliminary cluster cutting analyses were conducted immediately after each recording session in order to identify units that were visually responsive and showed orientation selectivity. Furthermore, in order to be included in the dataset the unit's average firing rate had to be larger than 0.15 Hz. After cluster cutting, 232 units recorded from four rats were included in the analyses, all of which were recorded over several sessions during both sessile and active behavior. Based on these criteria and the time available for my master thesis, data from eight of the animals were excluded from further analysis in the thesis but will be included when the work is prepared for publication.

Quantification of data is mostly presented as "box and whisker" plots. The box includes the 25^{th} to the 75^{th} percentiles and whiskers are drawn from the 10^{th} to 90^{th} percentile. The midline of the box, and error bars indicate the median and standard deviations, respectively. Results in the text are given as mean±SEM with "n" referring to the number of units.

3.1 Methodological assessment

3.1.1 The impact of tetrode implants and microinjection on neurons

In order to verify the position of the recording electrodes and the depth of the recording sites, sections were stained for Nissl bodies, which label cell soma of neurons. This also enabled us to assess possible damage to the tissue due to the surgical procedure of implanting the tetrodes or when lowering the tetrodes during the experimental period. In seven of the twenty-four hemispheres recorded from we could observe minor damage to the top of the cortex, but there were no indications that this affected the behavior of these twelve animals or the number of units recorded in the electrophysiological recordings. The tetrode tracks can be detected

due to slight displacements of the tissue and necrosis in the middle of the track (Figure 3.1A). For the tracer injections, all sections at the injection site were examined to verify injection coordinates and to reveal tissue damage caused by the injection. Based on both the injection sites, as well as the areas that were labeled by tracers (section 3.4), we concluded that the stereotaxic coordinates targeted the brain areas we aimed for; dLGN and V1. No tissue damage was observed at the area labeled by tracers, which was expected as the anterograde and retrograde tracers were injected *at least* 1 mm anterioposterior to the brain area of interest.

3.1.2 Histological verification of recording location

It was assumed that the tetrodes were located in the deeper layers of V1 when we terminated the electrophysiological experiments. To verify this, the depth was measured from high-resolution light microscopy images using the AxioVision software (Figure 3.1A). The depth from the top of the cortex, to the end of the tetrode track was measured to be 750-1850 µm with an accuracy of approximately ±100 µm (Figure 3.1B). Comparing these measurements with the notes from the laboratory protocol on how much the tetrodes were lowered during experiments, it was calculated that the 232 units included for further analysis were recorded from tetrode depths between 550-1850 µm which corresponds to L2/3, L4, L5 and L6. Units showing motion resistance, to be described in the following sections, were recorded between approximately 1200-1800 µm which is in accordance with cell layers 5 (L5) and 6 (L6) of the V1 in rats (Paxinos & Watson, 2007; Zarrinpar & Callaway, 2006). The anterioposterior and mediolateral coordinates were too few and variable to investigate if the MROS units were confined to a specific location in V1. Sections with tetrode tracks from animals used in the analyses can be found in appendix 6.4.

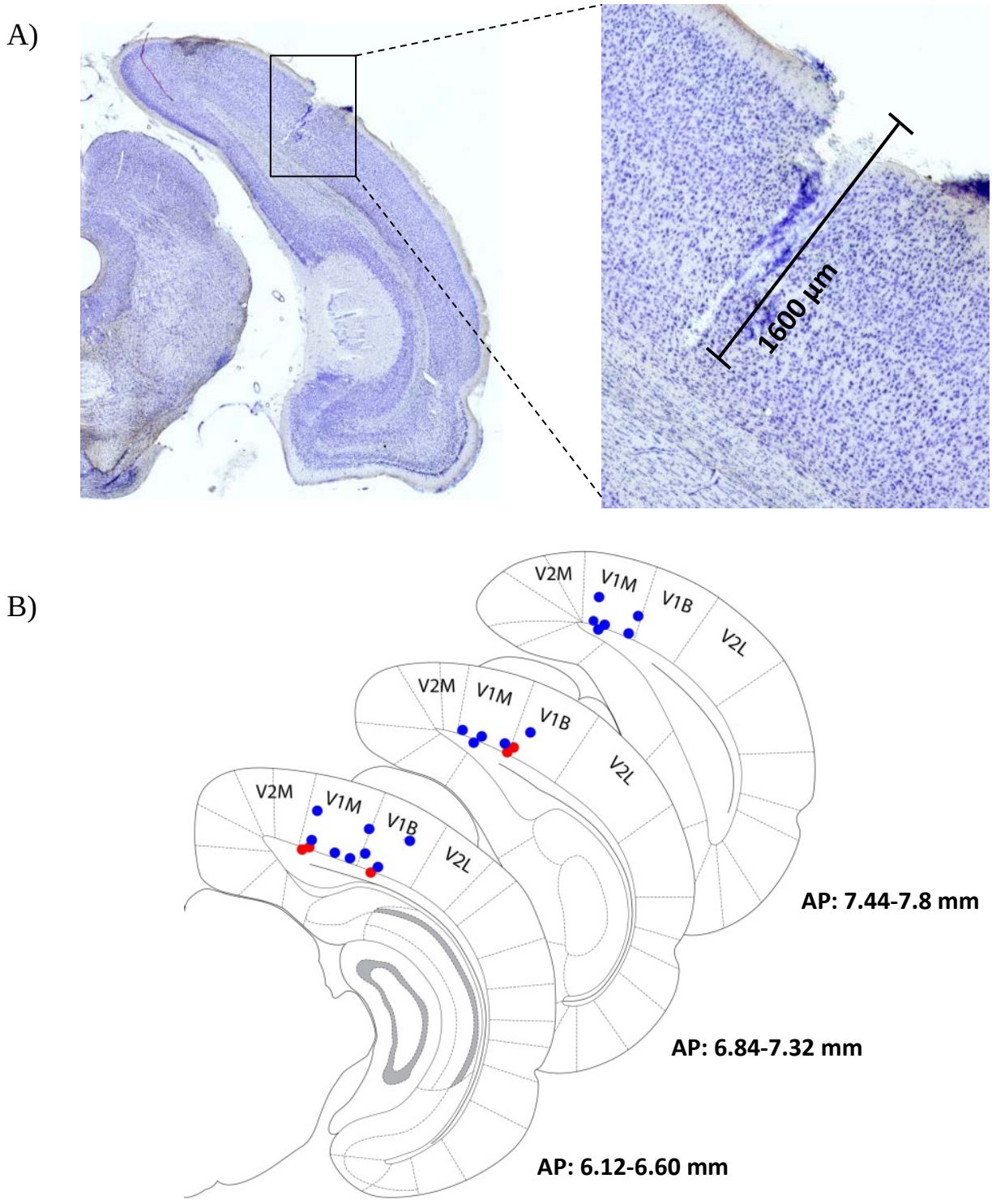

Figure 3.1: Histological verification of tetrode position of twelve rats, twenty-four hemispheres. A) Nissl-stained coronal brain section showing the tetrode track. Scale bar is the measurement of the tetrode track in cortex. B) Sketch of coronal sections modified from Watson and Paxinos (2007), indicating the areas of the visual cortex with the end-point of tetrode tracks from all animals superimposed (red and blue dots). The anterioposterior (AP) position is relative to bregma (posteriorly). The five red dots indicate the end-point of the tetrodes where we found movement resistant orientation selective (MROS) units and the 19 blue dots represent end-points where MROS units were not found.

In order to visualize cortical layers, dual fluorescent staining with anti-PCP4 and Nissl was used (Figure 3.2). Anti-PCP is a reliable marker of neurons in the deeper layers of V1 (Watakabe et al., 2012). The staining of PCP4 was strong in L5 and L6, but weak in superficial layers. This separation into layers was compared with the tetrode tracks in order to identify the layer from which the recordings were conducted (Figure 3.2C).

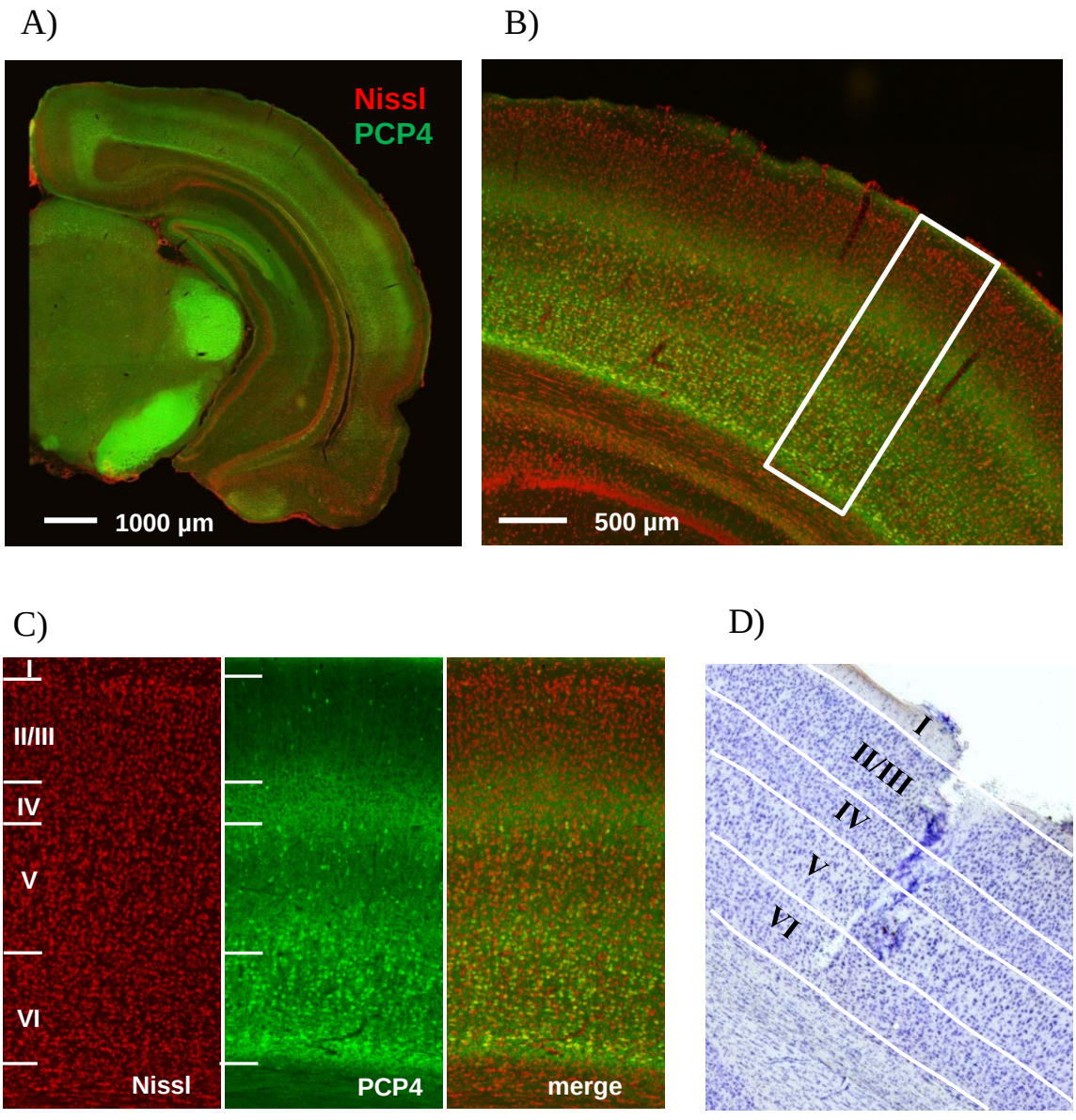

Figure 3.2: Coronal section with fluorescent labeling of (A) PCP4 and Nissl bodies and (B) an image of V1 of higher magnification. C) Cortical layers with anti-PCP4 staining and fluorescent Nissl staining. D) Same image as in Figure 3.1A, but separated into layers based on the dual fluorescent staining in C.

3.1.3 Behavioral conditions

The tracking data was analyzed based on path length, trajectory plots and occupancy maps to determine if a recording could be characterized as “sessile recording” or “movement recording” (Figure 3.3). The box was divided into 11 segments, and for a session to be categorized as a sessile recording, the animal would have to have more than 80 % of its movement restricted to one to three adjacent segments. Other recordings were characterized as movement recordings. The average data from the two sessions with the least movement, and the two sessions with the most movement, were used for classifying subgroups of neurons and for analyzing orientation selectivity and neuronal activity.

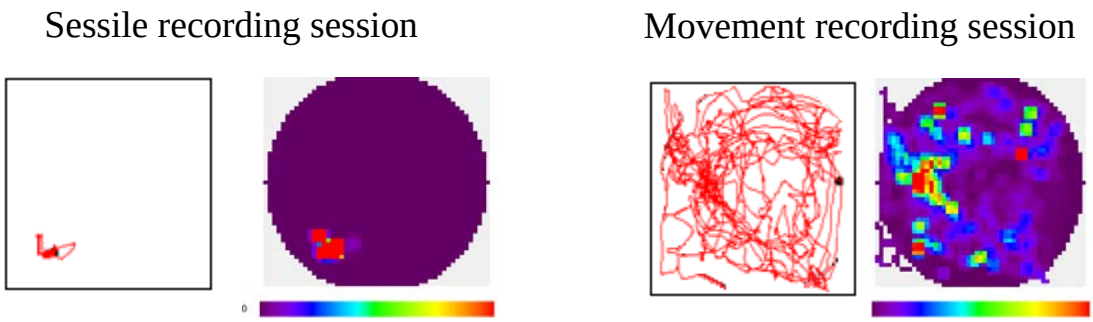

Figure 3.3: Summary of overhead tracking in two sessions from the same animal demonstrating behavioral conditions for sessile recording session (left panel) and movement recording session (right panel). Trace of the rat’s trajectory (red line, left panels) in the recording box and a color coded occupancy map of the recording box (right panels; fraction of time spent in each bin from not visited (blue) to largest fraction of time (red)) in two sessions representing a session where the rat was sessile (left panel) and active (right panel). This was used together with path lengths and segment analysis to determine the behavioral conditions.

3.2 Classification of units into different subgroups

3.2.1 Classification of units based on waveform parameters

The neuron population in V1 is made up of approximately 15-20 % inhibitory neurons and 80-85 % excitatory neurons (Markram et al., 2004). Inhibitory neurons have been shown to have low orientation selectivity in V1 of rodents (Kerlin et al., 2010; Niell & Stryker, 2008) and should be treated as a separate group. In order to isolate putative inhibitory neurons, we

separated units based on features of the unit's waveform. Inhibitory units have been shown to have shorter peak to trough period, and a narrow spike width (half-amplitude time (Niell & Stryker, 2008). The half width of the amplitude was compared with the peak-to-trough duration (see section 2.6.2, Figure 2.5) in a scatterplot (Figure 3.4). The waveforms were manually inspected for all units within the lower cluster and units close to them, and labeled as putative inhibitory or excitatory. In total 36 units (16 % of the population) were labeled as putative inhibitory units and excluded from further analysis, which then included 196 neurons.

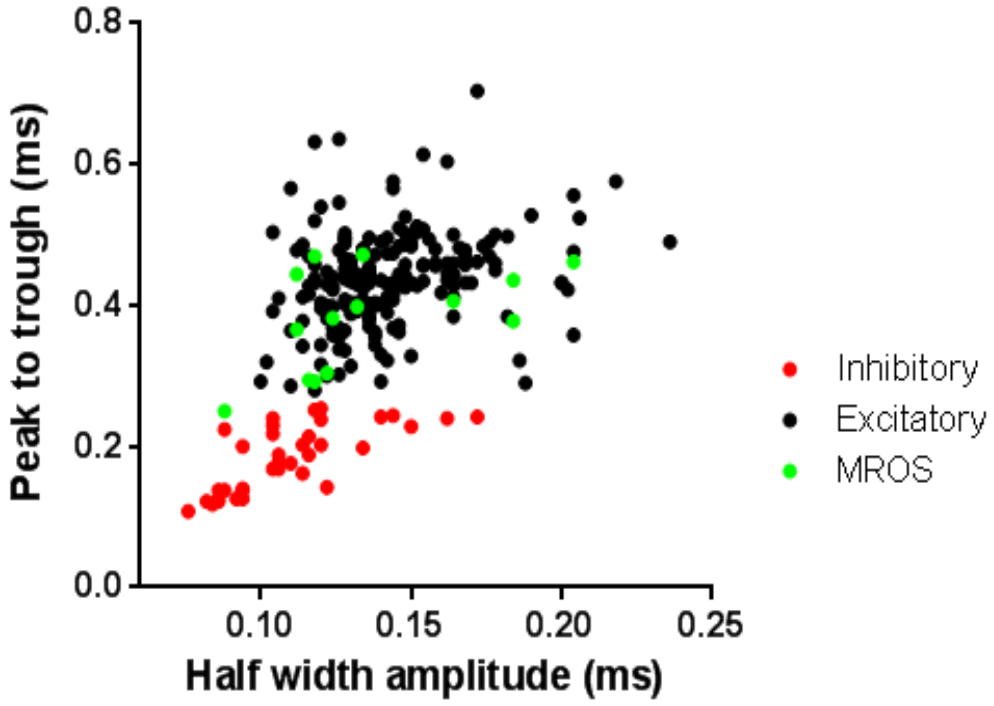

Figure 3.4: Classification of excitatory and inhibitory units using waveform analysis. The units were separated based on the half width of the amplitude and peak-to-trough duration, where the inhibitory neurons (red) clustered at the lower values in the scatterplot. Sixteen percent of the cell population was classified as inhibitory units. Movement resistant orientation selective (MROS) units (explained in the following section) were also labeled (green), but did not differ in waveform from other excitatory neurons.

3.2.2 Tuning properties of neurons in V1

Preliminary analyses were performed between sessions to determine if the cells were orientation selective (OS) or not. The raster plots, tuning curves and orientation selectivity index (OSI) were calculated for all units. The closer the OSI is to 1, the more selective the unit is. If a recording from a sessile animal contained neurons with strong response to one orientation and with an OSI higher than 0.5, additional recordings where the animal was actively moving were conducted to investigate the effect of movement on the neurons' response patterns. We found orientation tuned units in all layers, but during animal's self-movement, the response to their preferred orientation was mostly less prominent or disrupted (Figure 3.5A). In some cases, the orientation preference would change between sessile recordings (Figure 3.5B). Overall, the majority of orientation selective neurons showed unreliable responses during self-movement. However, in a subpopulation of units, the orientation preference remained stable across several sessions of both sessile and active behavior (Figure 3.5C). We termed these units movement resistant orientation selective (MROS) neurons, and as our investigation show, these units appear to be confined to L5 and L6.

A)

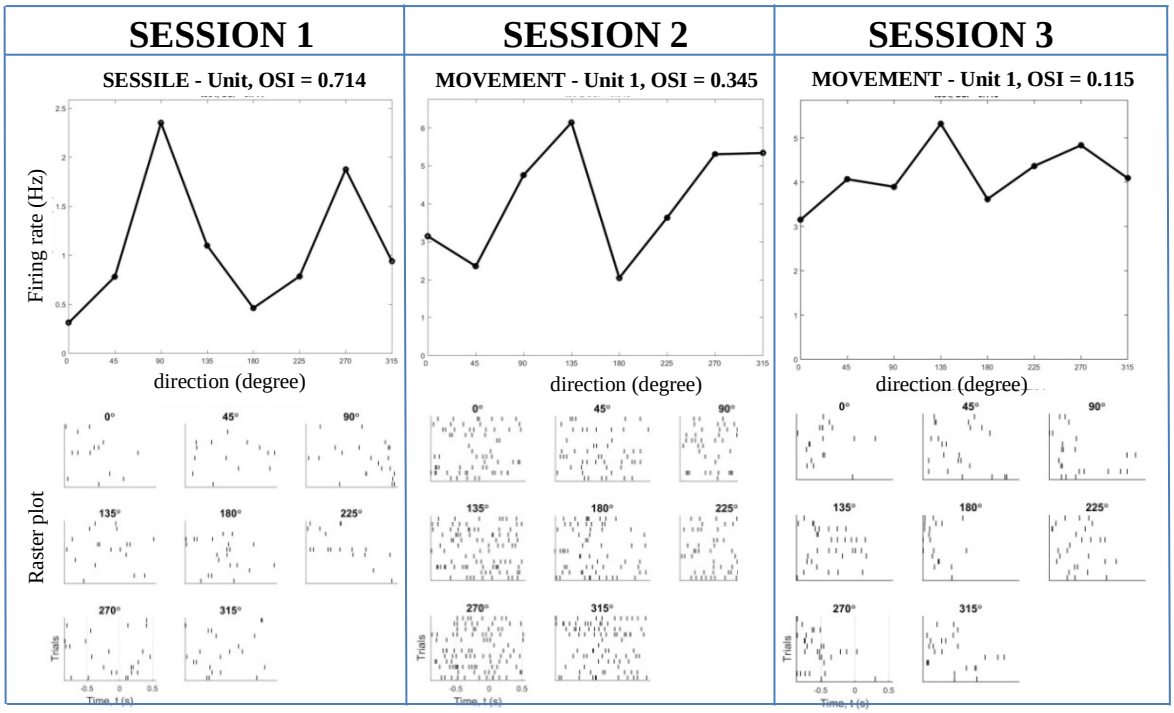
SESSION 1
SESSION 2
SESSION 3
SESSILE - Unit, OSI = 0.714
MOVEMENT - Unit 1, OSI = 0.345
MOVEMENT - Unit 1, OSI = 0.115
Firing rate (Hz)
direction (degree)
Raster plot
0°
45°
90°
135°
180°
225°
270°
315°
Trials
Time, t (s)

B)

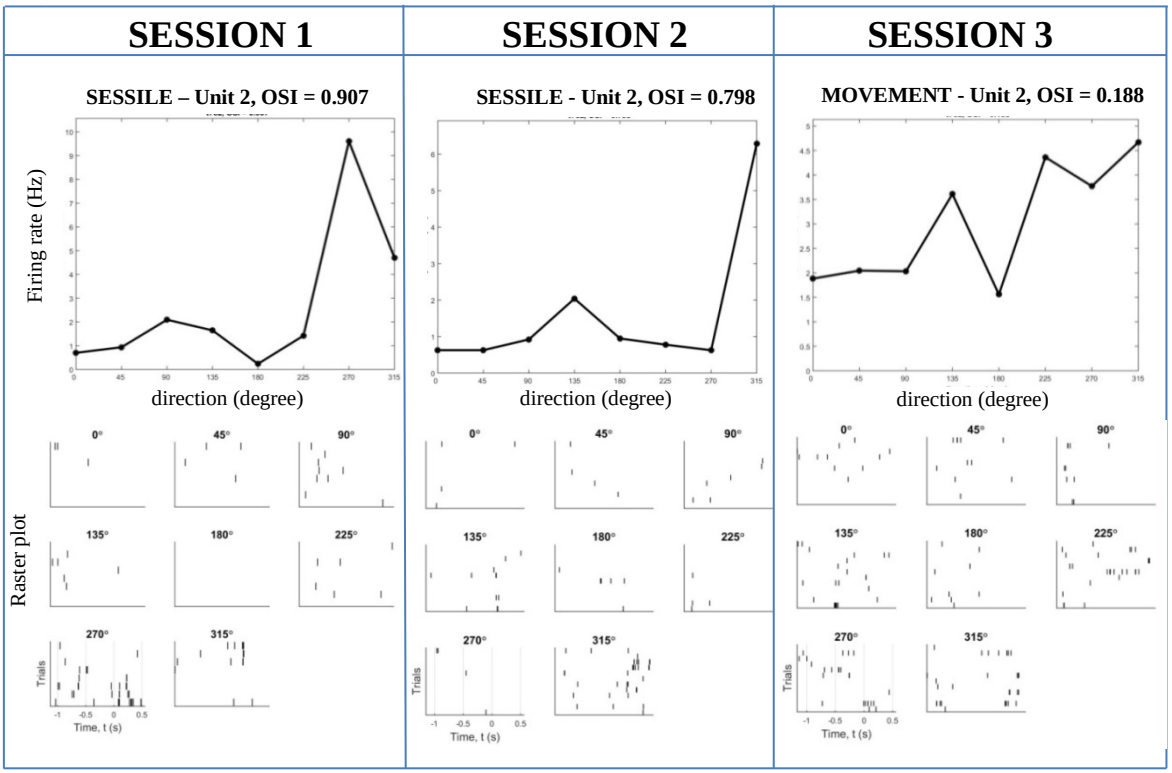
SESSION 1
SESSION 2
SESSION 3
SESSILE – Unit 2, OSI = 0.907
SESSILE - Unit 2, OSI = 0.798
MOVEMENT - Unit 2, OSI = 0.188
Firing rate (Hz)
direction (degree)
Raster plot
0°
45°
90°
135°
180°
225°
270°
315°
Trials
Time, t (s)

C)

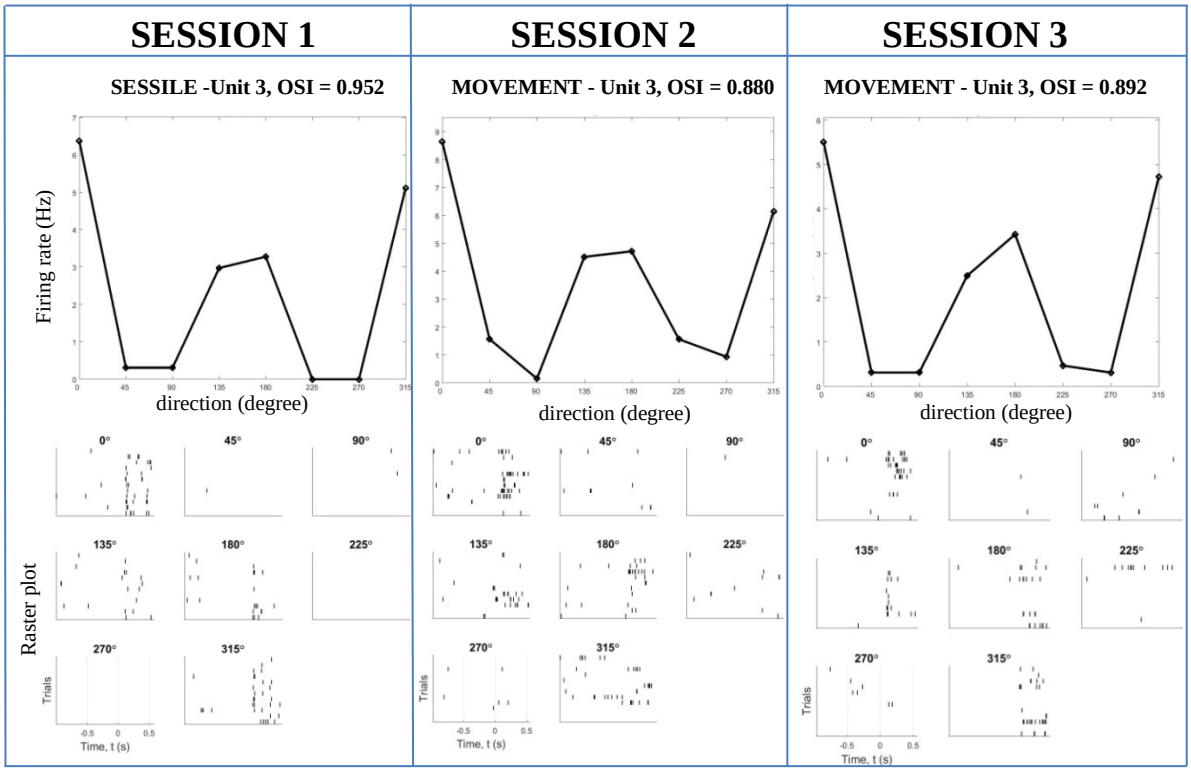

Figure 3.5: Orientation selective units respond differently to the animal's self-motion. Tuning curves and raster plots for three units (A, B, C) and their responses to visual stimuli presented at eight different orientations and repeated twelve times. A) Orientation tuning curves from a unit recorded in L5 across three sessions. In session 1 (sessile behavior; left panel) the unit responds to horizontal gratings moving up (90˚) or downwards (270˚) on the screen and show a high orientation selectivity index (OSI=0.714). In session 2 and 3 (active behavior; right panels), the overall firing rate is higher, but unspecific, hence the unit has lower OSI (0.345 and 0.115). B) Orientation tuning curves from a unit recorded from L4 across three sessions. The orientation preference of the unit changes from one sessile recording to the next (session 1 (90˚/270˚) compared to session 2 (135˚/315˚)). The orientation selectivity was disrupted during movement (session 3). C) Orientation tuning curve of a movement resistant orientation selective (MROS) unit from L6. The orientation preference remains stable across both sessile recordings (session 1) and recordings with movement (session 2 and 3).

3.2.3 Characterization of subgroups based on orientation selectivity

To investigate if the MROS units represent a separate functional group classified and separated from other units based on OSI between sessile and moving state, the average OSI of 196 units was compared. The average OSI of units from two consecutive movement recording sessions was compared with the average OSI of units in two sessile recordings (Figure 3.6).

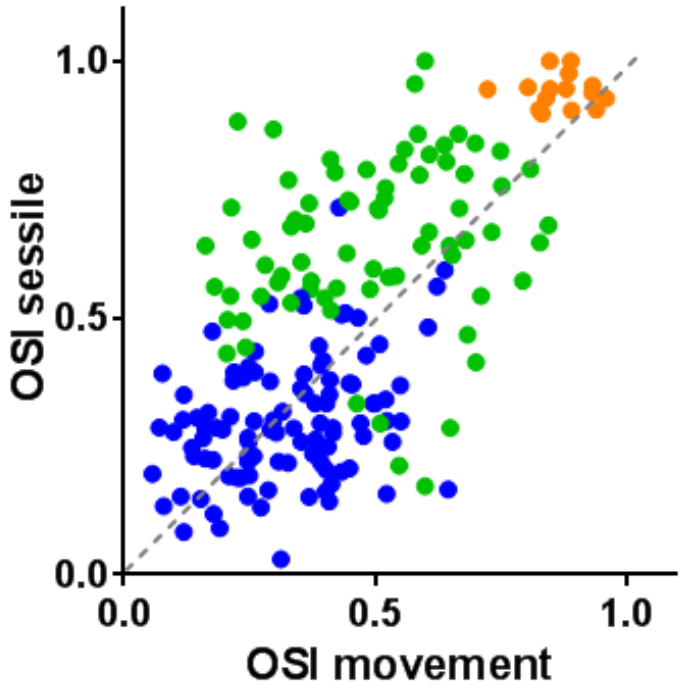

Figure 3.6: Scatterplot comparing orientation selectivity index (OSI) of units recorded while the animal was either sessile (OSI sessile) or moving around (OSI movement) (n=196 units). Units clustering at higher OSI values (OSI sessile>0.90 and OSI movement>0.75) were classified as movement resistant orientation selective units (MROS, orange, n=15). Units that displayed orientation selectivity in their tuning curves, and had OSI>0.45 in either sessile or moving conditions, were classified as orientation selective units (OS, green, n=75). Other excitatory units with no apparent preference in tuning curves, and OSI<0.45 were termed other excitatory units (OE, blue, n=106). Some units had OSI>0.45, but had no apparent orientation preference, these were also classified as OE units.

Units with stable orientation tuning during movement and sessile recording sessions were close to the dashed line. A subpopulation of neurons, MROS units, showed exceptional orientation tuning stability across sessile and moving behavior. A prominent feature of these MROS units was remarkably sharp tuning curves for the preferred orientations in both sessile

and active behaviors compared to other units. They also seem to separate out at higher OSI (OSI sessile above 0.90 and OSI movement above 0.75, Figure 3.6). In order to compare the MROS units with other orientation selective (OS) units, a threshold of OSI>0.45 during sessile recordings was chosen to be classified as OS units. This was the lowest OSI value where we could detect clear orientation tuning in the tuning curves by manual inspection. There were some exceptions to this as some cells displayed increased OSI values during movement, and these were also classified as OS cells if OSI>0.45. The OSI measure is not sensitive to shifts in orientation preference across recording sessions. Therefore, two additional criteria were included where (1) the preferred orientation in tuning curves had to be stable in at least two sessile recording sessions with (2) a mean firing rate above 0.15 Hz in order to exclude units with high OSI due to a few random spikes that coincidentally occurred at a specific orientation. The latter criterion was applied for all units recorded. Units with an OSI below 0.45 was categorized as “other excitatory” (OE) neurons. In Figure 5 there are some OE neurons with OSI>0.45. However, these units were not orientation tuned in the tuning curves, hence classified as OE neurons. In accordance to these criteria, the population was separated into 15 MROS cells, 75 OS cells and 106 OE cells (Figure 3.6).

While MROS units were quite uniform in regards to tuning curves and raster plots, the two other groups were highly variable. In order to rule out that circumstantial conditions were responsible for the variety of responses, we chose to compare MROS units to simultaneously recorded units from the very same session. This ensured that the recording conditions were identical for all units used in further analysis. Among the simultaneously recorded units we found variable responses in orientation tuning in response to movement. Some units remained stable across behavioral conditions while other units recorded simultaneously and also from the same tetrodes, showed profound changes in their response pattern even though less than 50 µm separates some of the electrodes from which the units were recorded (Figure 3.7).

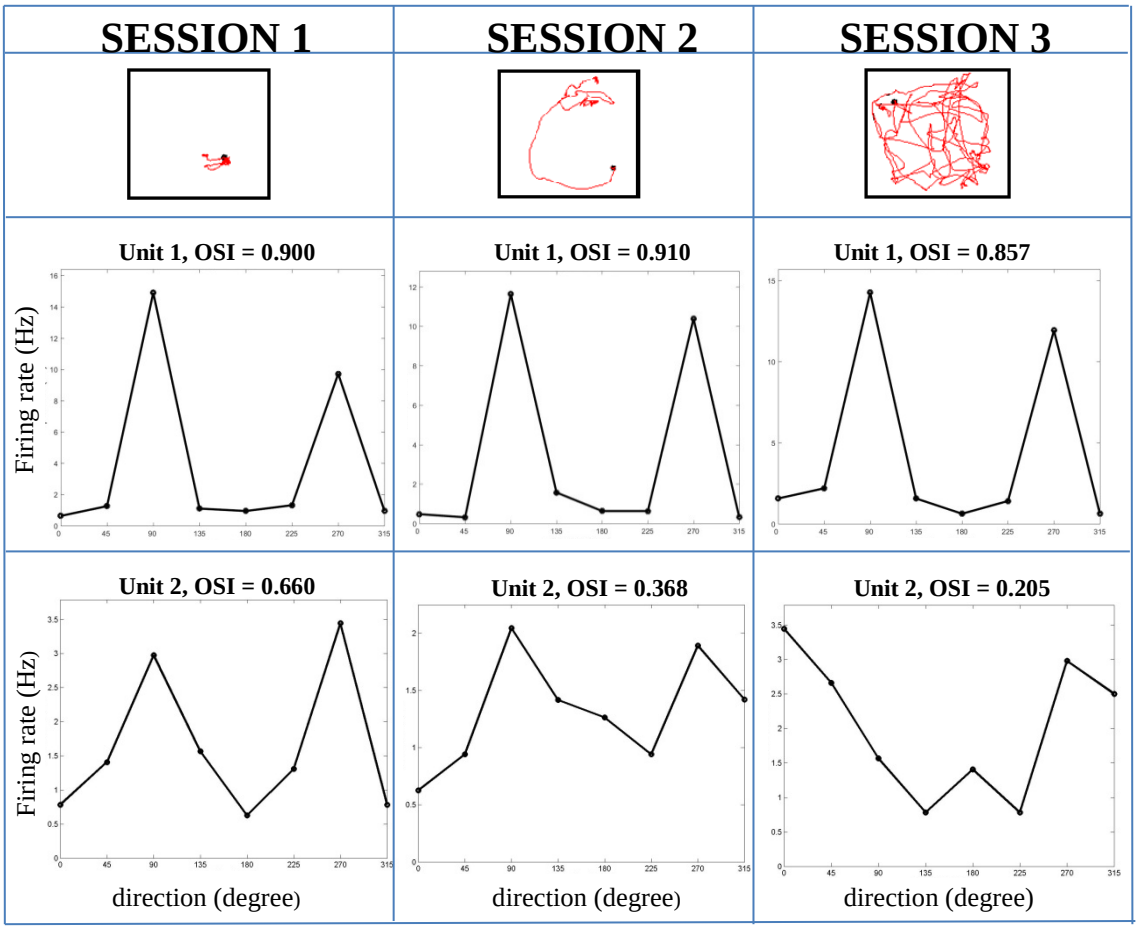

Figure 3.7: Different effect of movement on orientation tuning in simultaneously recorded neighboring units from L5/L6. Top panel shows the path (red trace) of the animal during sessions. The middle panel shows the tuning curve of a movement resistant orientation selective (MROS) neuron (Unit 1) which is stable across sessions despite the animal spending a large amount of time moving around in the enclosure. The lower panel shows tuning curves from a simultaneously recorded orientation selective (Unit 2) neuron from the same tetrode, where OSI is decreased with movement (OSIsessile= 0.66, OSImovement= 0.20).

The simultaneously recorded units (n=120 neurons) were then compared and classified based on OSI (Figure 3.8).

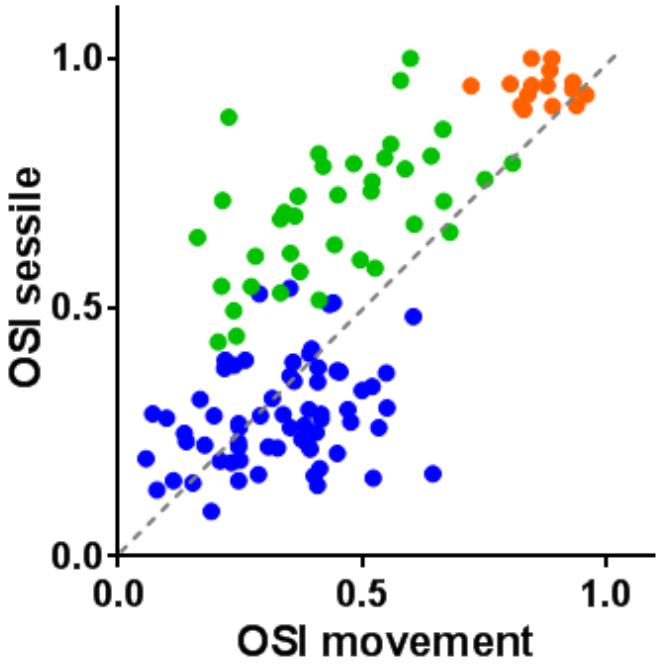

Figure 3.8: The population of units recorded simultaneously with movement resistant orientation selective (MROS) neurons. The scatterplot compares OSI of all units (n=120) from recording sessions with sessile behavior (OSI sessile) and movement (OSI movement). Units with OSI sessile>0.90 and OSI movement>0.75 were classified as MROS neurons (orange, n=15). Units with OSI sessile>0.45 was classified as OS neurons (green, n=38). The remaining units were categorized based on OSI<0.45 in sessile recordings and were the grouped as OE neurons (n=67) represented in blue. Orientation selective units have a significantly higher OSI in sessions when they are sessile compared to moving (MROS and OS combined, n=53, OSI sessile/movement: 0.76±0.02 / 0.57±0.03, $p<0.0001$, paired t-test applied).

Based on the above mentioned criteria, the simultaneously recorded units seem to separate into three subpopulations based on their OSI and stability of the OSI across behavioral states: 15 MROS neurons, 38 orientation selective (OS) neurons, and 67 other excitatory (OE) neurons. Most orientation selective neurons have a higher OSI in sessions where the animals are sessile compared to moving. To test this, we compared the OSI during movement and sessile recordings for all orientation selective units (MROS and OS), and found a significant difference in OSI between the two states (OSI sessile/movement: 0.76±0.02 / 0.57±0.03, $p<0.0001$, paired t-test applied).

3.3 Functional properties of MROS and simultaneously recorded units

3.3.1 Orientation selectivity

Orientation selective cells showed a significant reduction in OSI during movement ($p<0.0001$, Figure 3.8). To further investigate how movement affects the orientation selectivity of each subgroup from sessile to moving state, the OSI of units within the three groups was compared (Figure 3.9).

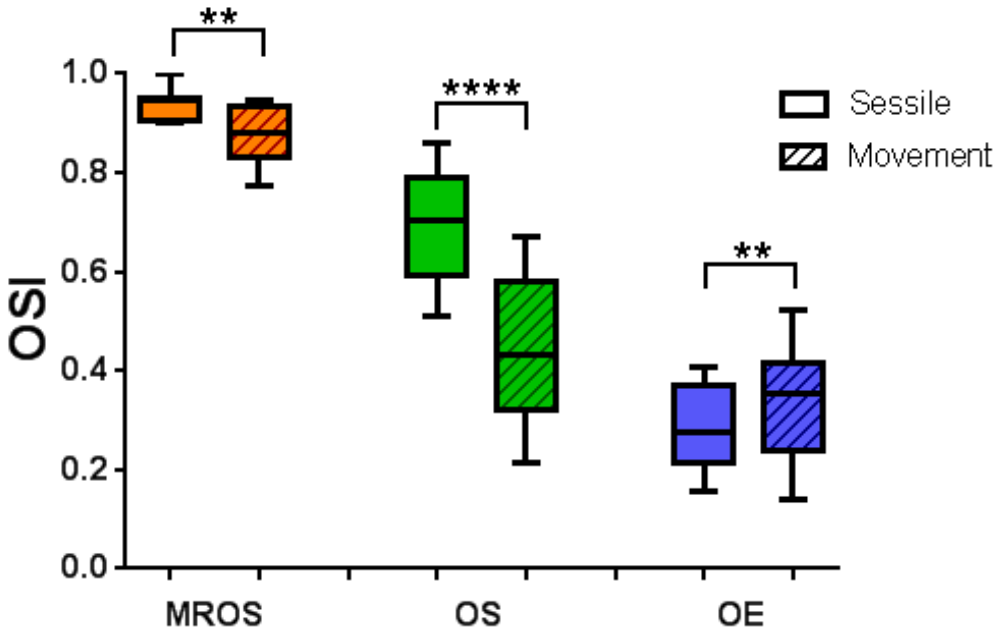

Figure 3.9: The OSI of the different groups from recordings where the animals were sessile compared to recordings with movement. There was a significant change in OSI from sessile to active behavior for all groups (MROS (n=15): p=0.0015, OS cells (n=38): p=0.0001, OE cells (n=67): p=0.0065, paired t-tests applied). There was also a significant difference across groups in both sessile and movement recordings (both $p<0.0001$, Kruskal-Wallis test). Furthermore, post-hoc analysis revealed that MROS and OS cells were not significantly different when the animal was sessile (p=0.062), but significantly different when the animal was moving ($p<0.0001$). Dunn's multiple comparisons test for subgroups in sessile state: MROS vs. OE: $p<0.0001$, MROS vs. OS: p=0.062, OS vs OE: $p<0.0001$. For moving state: MROS vs. OS: $p<0.0001$, MROS vs. OE: p=0.0001, OS vs. OE: p=0.026.

All groups had a significant change in OSI during movement (Figure 3.9), but the most apparent effect was found in OS cells with a 40 % decrease in mean OSI from 0.70 to 0.43 in during movement (MROS units (n=15): OSI sessile/movement= 0.94±0.0008 / 0.86±0.02, p=0.0015. OS units (n=38): OSI sessile/movement= 0.70±0.02 / 0.43±0.03, p=0.0001. OE units (n=67): OSI sessile/movement= 0.29±0.01 / 0.34±0.02 p=0.0065, p=0.0065. Paired t-tests applied). We also compared the different groups in each of the two conditions, and found a significant difference in both sessile and movement recordings ($p<0.0001$ in both conditions, Kruskal-Wallis test), however, post-hoc analysis revealed that MROS and OS cells did not have significantly different OSI during sessile recordings (MROS vs. OE: $p<0.0001$, MROS vs. OS: $p=0.062$, OS vs OE: $p<0.0001$, Dunn's multiple comparisons test). During movement recordings, all groups were significantly different from each other (MROS vs. OS: $p<0.0001$, MROS vs. OE: $p=0.0001$, OS vs. OE: $p=0.026$, Dunn's multiple comparisons test), and the mean OSI was twice as high in MROS neurons (mean OSI= 0.86) compared to OS neurons (mean OSI= 0.43). Furthermore, there was a significant difference in the actual change in OSI from sessile to movement across groups (MROS change in OSI: ÷0.072±0.02, OS change in OSI: ÷0.25±0.02, OE change in OSI: 0.050±0.02, $F=55.23$, $p<0.0001$, one-way ANOVA), and post-hoc analysis revealed that there was a significant difference between all groups (MROS vs. OS: $p=0.0002$, OS vs. OE: $p<0.0001$, OE vs. MROS: $p=0.0077$, Tukey's multiple comparisons test).

Taken together, the results show that all groups are significantly affected by movement, but while MROS and OS cells have similar properties with regards to OSI during sessile behavior, the OSI is greatly reduced in OS cells during movement, while MROS remain highly selective. Additionally, the actual change in OSI from sessile to moving behavior was significantly different between groups and more than three times larger in OS units compared to MROS and OE units.

3.3.2 Evoked and spontaneous firing rates

In order to investigate whether the differences between the subgroups in sessile OSI and the different responses in OSI during movement was reflected in other properties, stimulus evoked and spontaneous firing rates were compared. The firing rates of neurons have been shown to increase during movement (Niell & Stryker, 2010). We therefore compared firing rates of the recorded units in sessile versus movement recordings (Figure 3.10).

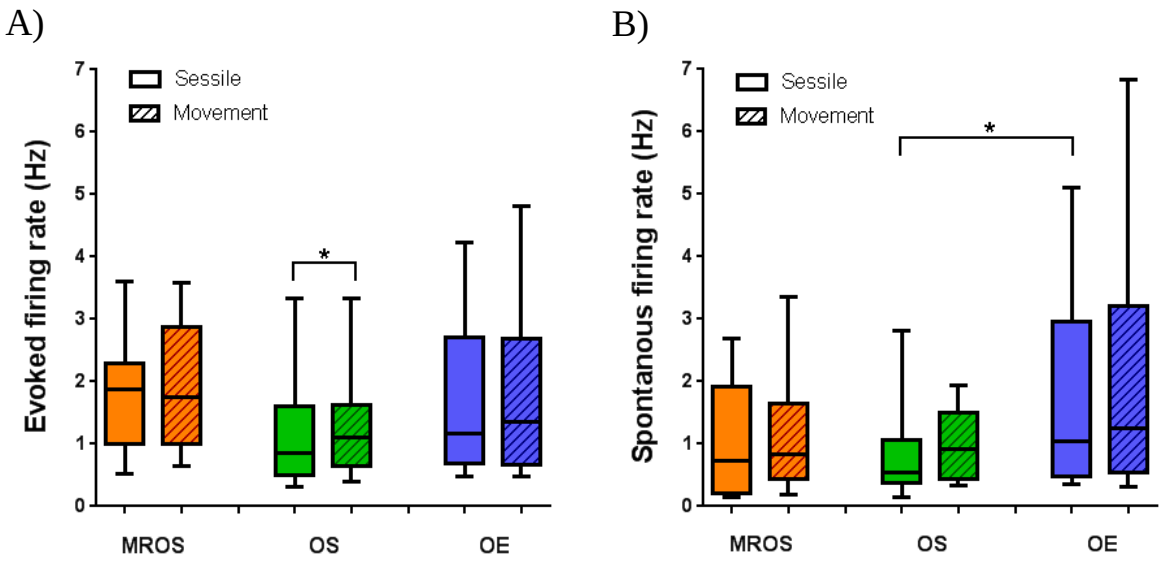

Figure 3.10: Stimulus evoked and spontaneous firing rates during recordings with sessile behavior and movement. A) Evoked rates for MROS, OS and OE neurons (n= 15, 38 and 67 units, respectively). There was a significant difference across groups for sessile recordings (p=0.038, Kruskal-Wallis test), but not for movement recordings (p=0.16 Kruskal-Wallis test). The results also revealed a significant increase in evoked rate during movement in OS neurons compared to sessile behavior, but not for MROS or OE cells (MROS: p=0.74, paired t-test. OS: p=0.040 and OE: p=0.78, Wilcoxon signed rank tests). B) Spontaneous firing rates of MROS, OS, and OE neurons. There was a significant difference across groups for sessile recordings (p=0.013, Kruskal-Wallis test), and post-hoc analysis revealed a significantly higher spontaneous firing rate in OE neurons compared to OS neurons (p=0.015, Dunn's multiple comparisons test). However, there were no significant differences in movement recordings (p=0.12, Kruskal-Wallis test). The changes in firing rates within groups were not significant (MROS: p=0.56, paired t-test. OS: p=0.059 and OE: p=0.21, Wilcoxon signed rank tests).

The evoked firing rates in sessile recordings were significantly different between all groups (p=0.038, Kruskal-Wallis test), however, there were no significant differences in evoked firing rates during movement (p=0.16, Kruskal-Wallis test) (Figure 3.10A). We also observed a significant increase in the evoked firing rate for OS neurons from sessile to movement recordings (OS units: evoked rate sessile/movement: 1.23±0.2 Hz / 1.47±0.3 Hz, p=0.040, Wilcoxon signed rank test). It cannot be ruled out if the observed increase is due to an overall increase in firing rates (see Figure 3.11 below). There were no significant increases in evoked rates for MROS and OE neurons during movement (MROS units: evoked rate sessile/movement: 1.85±0.3 Hz / 1.92±0.3 Hz, p=0.74, paired t-test. OE units: evoked rate sessile/movement: 1.90±0.2 Hz / 1.97±0.2 Hz, p=0.78, Wilcoxon signed rank test).

Analysis of spontaneous firing rates in sessile recordings revealed that there was a significant difference across all groups ($p=0.013$, Kruskal-Wallis test), and a post-hoc test showed that spontaneous rate in OE neurons was significantly higher than OS neurons (OE vs. OS: $p=0.015$, Dunn's multiple comparison test) (Figure 3.10B). There were no significant differences for movement recordings ($p=0.12$, Kruskal-Wallis test). Moreover, there were no significant changes in spontaneous firing rate from sessile to movement recordings within groups (MROS: spontaneous rate sessile/movement 1.11±0.3 Hz / 1.2±0.3 Hz, $p=0.56$, paired t-test. OS: spontaneous rate sessile/movement: 1.03±0.2 Hz / 1.24±0.2 Hz, $p=0.059$ and OE: spontaneous rate sessile/movement: 1.96±0.2 Hz / 2.14±0.3 Hz, $p=0.21$, Wilcoxon signed rank tests).

Even though it was not significant for all groups, movement tended to result in minor increases in the spontaneous firing rates, as well as an increase in the evoked firing rate for OS and OE neurons. When MROS neurons showed an increase in evoked rate, it was mostly observed as an increase at the specific angles they were selective for (Figure 3.11A), but as mentioned above, the increase in evoked rate for both OE and OS neurons during movement is most likely due to an overall increase in firing activity (Figure 3.11B). The evoked rate is simply measured as the firing rate after onset of stimulus which means that an overall increase in firing rate will lead to a rise in the evoked firing rate as well.

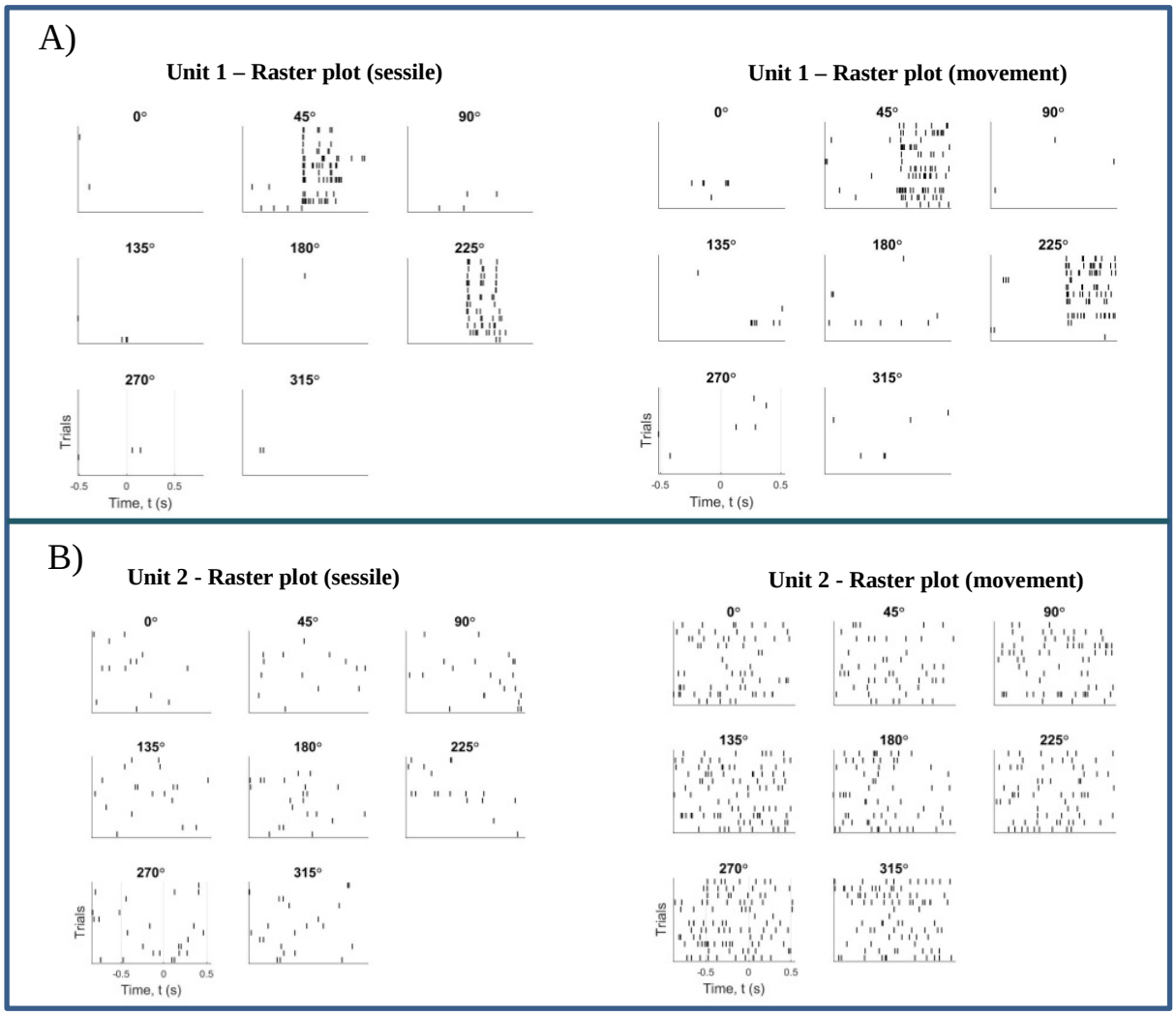

Figure 3.11: Evoked firing rates can either be due to increased visual response for preferred orientations or as a result of an overall increase in neuronal activity. A) Left panel: raster plot of MROS unit from sessile recording. Right panel: raster plot of MROS unit from movement recording with increased stimulus evoked response which is mostly specific for the unit's preferred orientation. B) Left panel: raster plot of an OS neuron from sessile recording. Right panel: raster plot of OS neuron from movement recording showing an unspecific increase in the overall firing rate.

To further investigate the properties of MROS neurons, the ratio between evoked and spontaneous firing rate was calculated for sessile and movement recordings, and compared (Figure 3.12). This would also show if the increase in evoked and spontaneous firing rates during movement was due to an overall increase in firing rates. Units with a ratio from zero to one had a higher evoked rate compared to spontaneous firing rate. Units with a ratio below zero had a higher spontaneous rate than evoked.

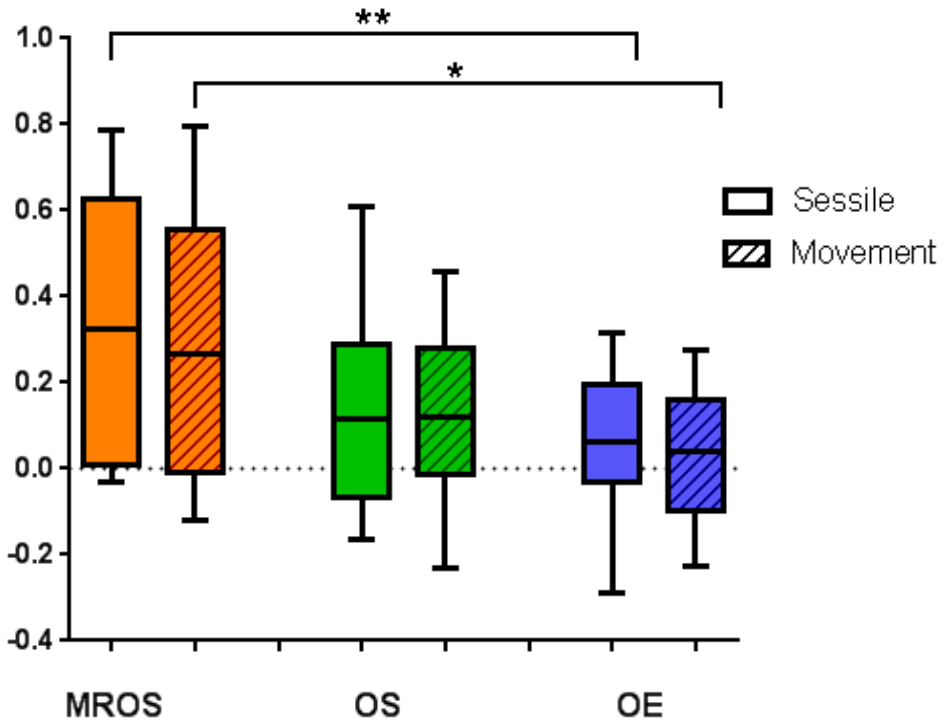

Figure 3.12: The ratio between evoked firing rate and spontaneous firing rate in the different groups. The ratio was calculated as $(R_{evoked} - R_{spontaneous}) / (R_{evoked} + R_{spontaneous})$, where R is the firing rate. There were no significant differences in ratio within groups (MROS (n=15): p=0.31, OS (n=38): p=0.27, OE (n=67): p=0.10, paired t-tests). However, there was a significant difference across groups in both sessile and movement recordings (sessile: F=5.8, p=0.0039, one-way ANOVA. Movement: p=0.0080, Kruskal-Wallis). Post-hoc analysis revealed a significant difference in ratio between MROS neurons and OE neurons for both sessile (p=0.0035, Tukey's multiple comparisons test) and movement recording (p=0.015, Dunn's multiple comparisons test).

Movement did not seem to affect the evoked/spontaneous ratio within groups as there were no significant differences (MROS: p=0.31, OS: p=0.27, OE: p=0.10, paired t-tests) (Figure 3.12). This suggest that the groups had either an equal rise in evoked and spontaneous firing rates which seems to be true for all groups, or that there was no change at all from sessile to movement. There was however a significant difference in evoked/spontaneous ratio across groups in both sessile and movement recordings (sessile: F=5.8, p=0.0039, one-way ANOVA. movement: p=0.0080, Kruskal-Wallis). Furthermore, post-hoc tests revealed that there was a significant difference between ratios in MROS and OE neurons in both sessile (p=0.0035, Tukey's multiple comparisons test) and active (p=0.015, Dunn's multiple comparisons test) behavior, but not between other groups. This means that the MROS neurons were not

statistically significantly different from OS neurons, but looking at the mean evoked/spontaneous ratio, the ratios were more than twice as high in MROS neurons (ratio sessile/movement: 0.32±0.08 / 0.28±0.08) than in OS neurons (ratio sessile/movement: 0.15±0.05 / 0.12±0.04), and more than triple the means of OE neurons (ratio sessile/movement: 0.06±0.03 / 0.03±0.03). Mean ratios suggest that a MROS neurons have a high evoked rate in relation to the spontaneous rate compared to other excitatory neurons.

3.4 Tracer injections to reveal connectivity

3.4.1 Retrograde tracing using cholera toxin subunit B injection

From histological inspection of the tetrode traces (Figure 3.2) it was revealed that the majority of MROS units were located in L6 in V1. Neurons in L6 is known to project back to the (dLGN). How this back-projection might modulate information conveyed through the dLGN to the visual cortex is unknown. As a first step to investigate if the MROS cells influence orientation tuning in the LGN, we examined the feedback projections from L6. The retrograde tracer Cholera Toxin Subunit B (CTxB) conjugated to AlexaFluor 594 was injected in the dLGN (Figure 3.13). In addition, the sections were stained for PCP4 in order to distinguish L6 from other cortical layers.

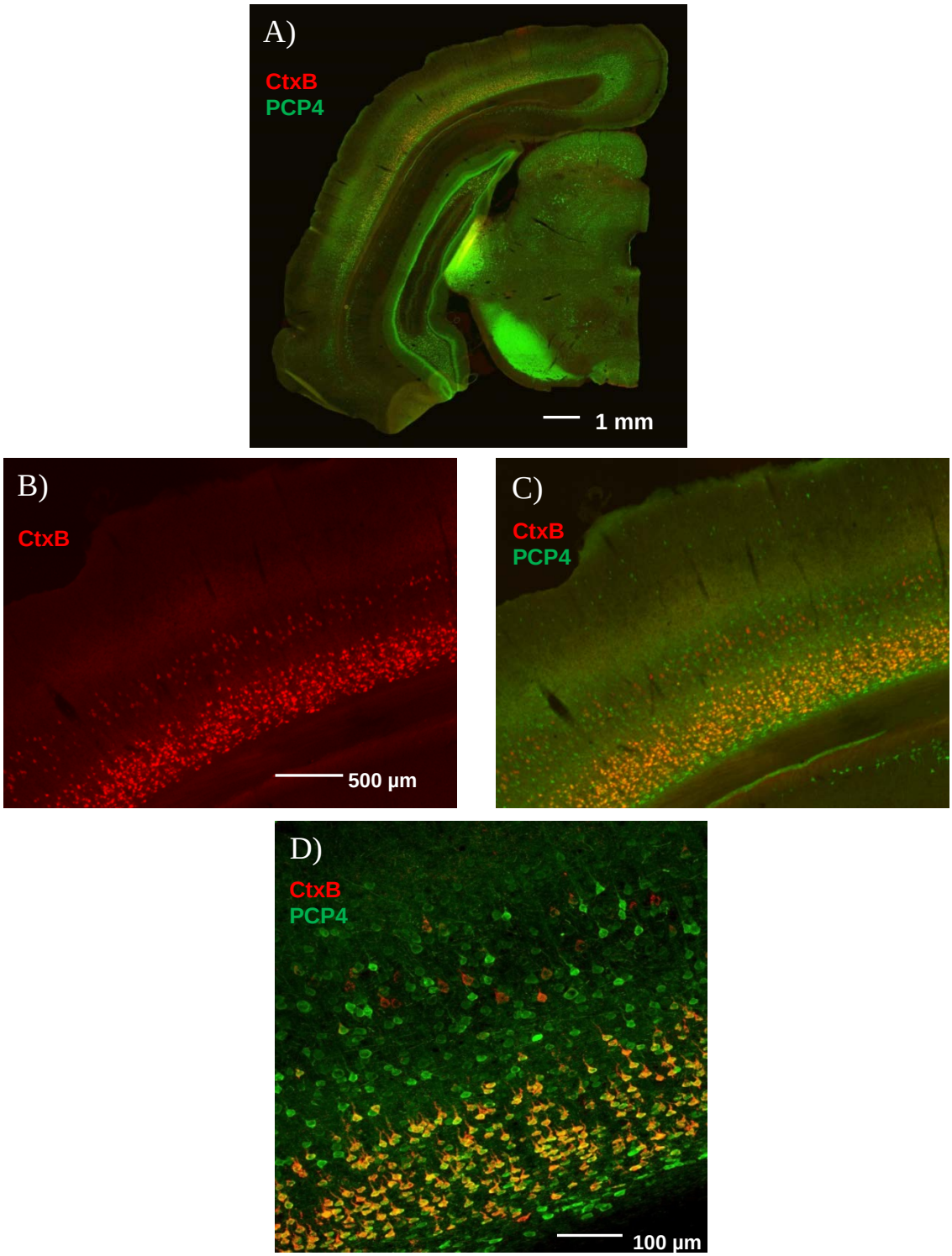

Figure 3.13: Neurons in layer 6 of the primary visual cortex (V1) project to the dorsal lateral geniculate nucleus (dLGN). A) Coronal section with fluorescently labeled cholera toxin subunit B (CTxB) and Purkinje cell protein 4 (PCP4). B) The retrograde CTxB (red) was injected in dLGN and transported back to L6 in V1. C) Image of CTxB labeled neurons in L6 (red) double-stained for PCP4 (green). PCP4-expressing neurons (green) co-localized with cortico-thalamic CTxB labeled neurons (red) in the upper area of L6 (L6a). The overlap is seen as yellow L6 neurons. D) Image of V1 with higher magnification of L5 and L6.

The L6 was strongly labeled by the CTxB. Interestingly, the PCP4-expressing neurons in the upper area of L6 (L6a) co-localized at large extent with the CTxB tracer, indicating that a substantial fraction of L6 neurons have cortico-thalamic projections (Figure 3.13). There were some CTxB labeled neurons in L5 as well, but these did not overlap with PCP4-expressing neurons indicating that they are likely a distinct population from the L6 cortico-thalamic cells. The injection coordinates aimed for dLGN, but seeing that some L5 neurons were labeled, the CTxB injection might have been a little deep and entered the top of vLGN where L5 neurons project (Deschênes et al., 1994).

3.4.2 Anterograde tracing with a viral vector

The MROS neurons seemed to be stable compared to adjacent excitatory cells, even though the recording conditions were the same. It may be that these neurons receive specific inputs or have a specific projection pattern but this is currently unknown. In order to explore the projection from deep layer neurons of V1 we used a viral vector (AVV5-Syn-ChR2-GFP) carrying Channelrhodopsin 2 (ChR2) and a green fluorescent protein tag (GFP) under a synapsin promotor for anterograde tracing. We did not make use for the ChR2 for optogenetic manipulations in the current study. The viral vector was injected into the deep layers of V1 (Figure 3.14).

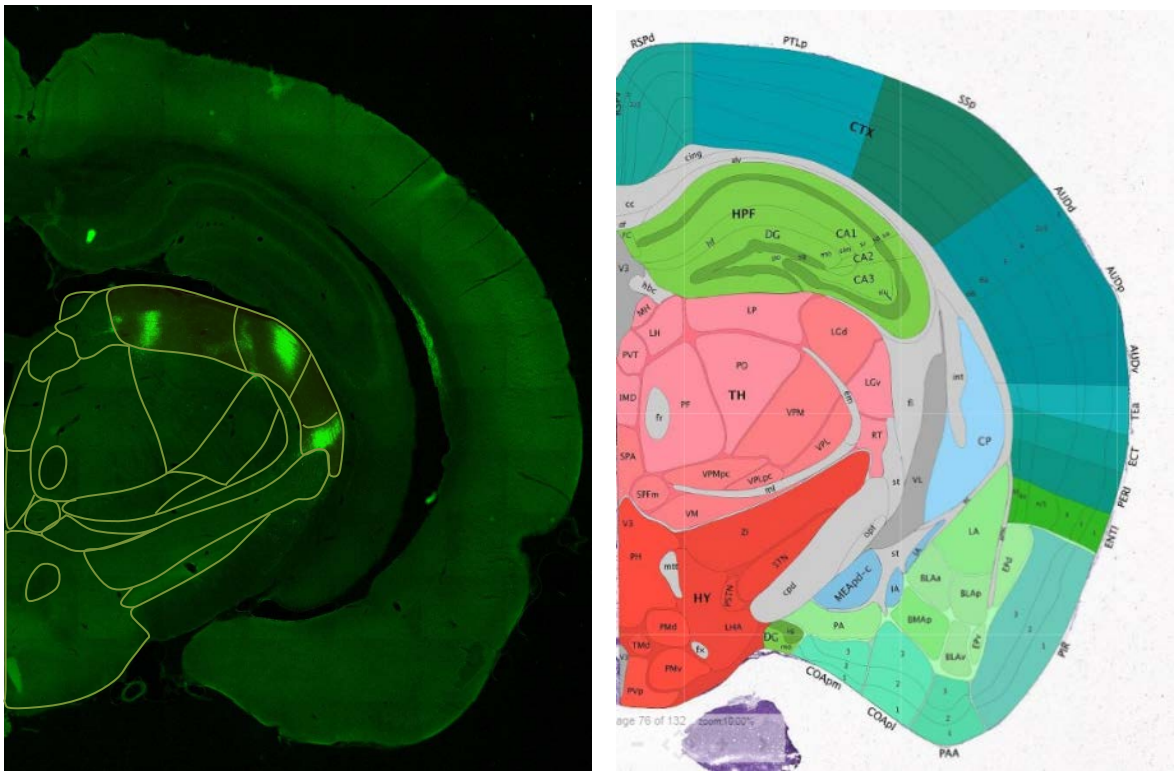

Figure 3.14: Anterograde viral vector injection in deep layers of the primary visual cortex (V1) showed fluorescent expression of projections in the dLGN. Left panel: Coronal section with labeling of the GFP tag on the expressed Channelrhodopsin 2. In addition to the dLGN, there was also expression in the lateral posterior nucleus (LP) and the thalamic reticular nucleus (nRT). Right panel: Sketch of a coronal section in mouse with different brain areas labeled. Modified from the data portal of the Allen Mouse Brain Atlas (2016)

As expected, the anterograde tracer terminated in the dLGN of the thalamus. Fluorescence expression was also observed in the thalamic reticular nucleus (nRT) and the lateral posterior nucleus (LP) (Figure 3.14). This is in accordance with earlier work on L6 projections (Bortone et al., 2014; Bourassa & Deschênes, 1995). It seems that the injection was local to L6, since leak into L5 would have resulted in viral expression in the vLGN as well as the lateral dorsal nucleus (LD) of the thalamus. These are areas L5 projects to in addition to the LP (Deschênes et al., 1994).

4 Discussion

In this study, we describe a subpopulation of excitatory units in the primary visual cortex of the rat which shows remarkable stable and highly selective responses to visual stimulation despite the animal freely moving. By use of single-unit extracellular recordings from about 800 neurons in freely moving rats we observed that of the 232 units used in further analyses, most orientation selective units (~85%) do not keep their selective orientation tuning when the animal was moving. However, a small fraction of the orientation selective units showed highly stable tuning curves, both during sessile and active behavior. These movement resistant orientation selective (MROS) neurons were found only in the deeper layers, mainly L6 of V1.

Retrograde tracing from the dLGN and anterograde tracing from L6 confirmed that the layers and area where the MROS units were found are reciprocally connected to the dLGN. This indicates that MROS neurons may have a function in modulating visual information already in the dLGN or through cortico-cortical interactions with other layers of the V1.

4.1 Methodological considerations

4.1.1 Electrophysiological recordings

There are several advantages of chronic recordings with multi-electrode recordings compared to single electrodes when assessing the neuronal activity in the brain. Firstly, the use of multi-electrode recordings in chronic experiments provides a mean to acquire large data-sets. The tetrodes used in these experiments allowed us to simultaneously record the activity of many units, and chronic implants enabled adjusting the depth to record from different cell layers over the course of the experiment. In addition to recording the activity of single units, multi-electrode recordings give insight into whole neuronal populations and the interplay within these microcircuits through local field potentials (Buzsaki, 2004). In contrast, single electrode experiments, performed with e.g. tungsten electrodes, have to be inserted at numerous locations in order to acquire datasets of similar magnitude. Additionally, such experiments are usually confined to acute preparation where the animal is anesthetized during the experiments, and sacrificed at the end of recordings. This excludes examinations of the effect

of behavioral states and movement, and limits the experimental recording period compared to experiments with chronic implants.

The chronically implanted tetrodes we used allowed the animal to move freely inside the box. Most studies considering V1 responses in awake animals have been restricted to head-fixed animals, which minimizes input from the vestibular system and effects of movement like head and body tilt. To the best of my knowledge, this is the first study to use chronically implanted tetrodes to investigate the effect of movement on the orientation selectivity in V1 of awake, freely moving rats.

However, chronic experiments with tetrodes are technically demanding, and there is a significant risk of tissue damage upon implantation. This could potentially lead to inflammation or the physical perturbation may influence the cortical microcircuit from which the recordings are being made. As an attempt to avoid the potential risk of tissue damage to the recording area, the tetrodes were usually implanted in an angle, meaning that lowering the tetrodes would move the tetrodes away from any damage. We observed tissue damage to the cortical surface in some of the stained brain sections, however, this was more likely due to the perfusion or sectioning procedure rather than from the surgery as similar damage could be seen outside the area where the tetrodes had been. There were no indications that this affected the animal's behavior or the number of units recorded.

Electrophysiological recordings provide excellent temporal resolution, but the disadvantage is that we cannot see the spatial distribution or the anatomical identity of the cells we are recording from. An alternative method would be to use high-resolution imaging, like for instance two-photon imaging, which allows for precise anatomical localization of the cells and simultaneous recordings of the activity of up to hundreds of neurons (Denk et al., 1990; Greenberg et al., 2008). However, most in vivo two-photon imaging studies are conducted in anesthetized or head-fixated animals, although miniature head-mounted two-photon microscopes have been created to allow for high-resolution brain imaging in freely moving animals (Helmchen et al., 2001; Sawinski et al., 2009). Another approach, which still is in the early days, are miniature fluorescence microscopes that can be mounted on the animal's head and allow for behaviors similar to my recordings. This could be a more fitting alternative for recording the MROS neurons observed in this study, but the temporal resolution is currently a limitation and methods development needed are substantial.

4.1.2 Spike sorting

The offline spike sorting is crucial in order to figure out which spikes are emitted from the same unit/neuron. Spike waveform change with the distance and relative position to the cell soma. In theory, the tetrode should be able to pick up spikes from about 1000 neurons at a radius of 140µm from the electrodes (Buszaki, 2004) but due to noise in the recordings and unknown factors we are mostly only able to adequately separate spikes from 5-20 units at one location. If the parameters of the waveform of two or several neurons overlap, and we could not separate the clusters of spikes, the data were excluded. Large amounts of data were left out for this reason. It is time consuming and challenging to identify units with overlapping clusters, thus we had to restrict the analyses to the units with clusters clearly separated from the noise or other activity. Moreover, the offline spike sorting is performed manually and could be subject to some degree of bias. To limit this, most of the spike sorting was done prior to any analyses of visual responses to limit the degree of bias.

4.1.3 Tracer injections

The most common method for microinjections is to do a single large injection with for instance Hamilton syringes with a tip diameter of 200-500 um. For the tracer injection, we chose to use the NanoJectII system with thin glass pipettes of a diameter of less than 15 µm, in order to minimize the tissue damage. The tracer was also injected in very small amounts in a step-wise manner to avoid too much spread across different layers.

4.1.4 Verification of recording location

From the histological examinations of the Nissl stained sections we found that the depth of the tetrode tracks ranged from 750-1850 µm into the cortex. The goal was to terminate the recordings when the tetrodes went through L6 and entered the corpus callosum, which has characteristic axon activity. The large range of tetrode end-points may indicate that the turning mechanisms of the microdrives were unreliable or that the dorsoventral measurements during implantation varied. However, in all experiments where we successfully recorded the MROS units the tetrodes ended up in the deeper cortical layers or the corpus callosum. Using the notes from the lab protocol on how much the tetrodes were lowered, it was calculated that all MROS neurons were recorded at cortical depths between approximately 1200-1800 µm, corresponding to L5 and L6.

The location of the MROS neurons in deeper layers raises some interesting theories since L5 and L6 are known to exhibit several distinct features of function and connectivity, which will be discussed further in chapter 4.5. The variation of anterioposterior and ventrolateral positions (Figure 3.1B) of the tetrodes in the Nissl stained sections was intentional to investigate if the MROS neurons were uniformly distributed in V1. From observations of the tetrode tracks, the MROS neurons seems to be distributed in both monocular and binocular areas, but it remains to be investigated if they are sparse and spread out across V1 or clustered at specific locations. However, they do not seem to be located too far posterior since we made no discoveries of MROS neurons here (Figure 3.1B).

4.1.5 Tracking and behavioral conditions

Tracking data was analyzed with analyseWM (Axona Ltd, Herts, UK). For the segment analysis, we set the limit to 80 % to include all recordings with MROS units. In future experiments, we hope to have sessile recordings where the animal is 100 % in one segment, and also movement recordings with better tracking, especially in regards to head movement to assess the effect of head tilt on orientation selectivity. Some data was excluded due to inconclusive tracking where we know from observational notes that the animal was sessile or active. Recent studies in mice V1 during locomotion show differences in the local field potential (LFP) in theta and gamma frequency ranges (Chen et al., 2015; Niell & Stryker, 2010) and such observations could give another mean of quantifying the behavior. If the behavioral state can be characterized by LFP responses it allows us to possibly include data where the over-head tracking was unreliable.

4.2 Classification of units into different subgroups

4.2.1 Classification of neurons based on waveform parameters

In the current study, neurons were classified as putative inhibitory or excitatory based on the spike waveform. In total 16 % of the total population of 232 neurons were classified as putative inhibitory neurons (Figure 3.4). Inhibitory neurons have been shown to sharpen the orientation tuning of cortical cells and affect the amplitude of the signals (Crook et al., 1998;

S. Lee et al., 2012; Liu et al., 2011; Shapley et al., 2003) but show low orientation selectivity (Kerlin et al., 2010; Niell & Stryker, 2008). While the interplay between inhibitory and excitatory neurons may be relevant in regards to the MROS neurons, for the scope of the current project, I chose to focus on the effect of movement on orientation selectivity and the functional properties of excitatory neurons. The putative inhibitory neurons were therefore excluded from the analyses in the current project.

4.2.2 Tuning properties of neurons in V1

To investigate the tuning properties of the cortical neurons recorded, the analyses were restricted to orientation selective cells across layers. We found different responses to visual stimulation across V1 (Figure 3.5) but did not observe any apparent layer-specific responses as described in previous studies (section 1.1.4). However, the majority of visually responsive units shared a common feature; their orientation selectivity was either reduced or disrupted during self-motion. The exception was the MROS neurons that had the same orientation preference across several sessions despite the animals' movement. This is, to the best of my knowledge, the first time such a property has been described in freely behaving animals. Our findings are in accordance with recordings from V1 in alert monkeys subjected to head tilts (Sauvan, 1999). In this study it was observed that other orientation selective neurons showed a type of constancy with regards to the retina, which means that the preferred orientation corresponded to the orientation as predicted from the body tilt and counter-rolling of the eyes (Sauvan, 1999). It is uncertain if the OS neurons we recorded acted in a similar way since the movement recording sessions did not have controlled head tilts and locomotion, but we did observe changes in preferred orientations during sessile recordings which might be a result of variation in head tilt between sessions (Figure 3.5B). However, while this cannot be concluded at this point, if MROS neurons are in fact the same type of neurons that Sauvan observed in monkeys, it is reasonable to believe that the MROS neurons' movement resistance, as well as the OS cells' instability is related to movement in direction of gravity, relative to body axis (like head tilts) and not the motor-related movement itself. This may also explain why studies in head-restrained animals report as much as 85-90 % of V1 neurons to be visually responsive (Niell & Stryker, 2010), while the yield in freely behaving animals, like in these experiments, is much lower due to uncontrolled head and body movement.

4.2.3 Characterization of subgroups based on orientation selectivity

The 232 neurons included in the analyses were separated into three groups based on their OSI during sessile and movement recordings; MROS, orientation selective (OS) and other excitatory (OE) neurons (Figure 3.6). MROS neurons constituted 6.5 % of the total population, which is in accordance with what Sauvan (1999) observed in V1 of monkeys (7% of V1 neurons). While this approach yielded a good separation of MROS neurons, the other groups were highly variable. For the rest of the analyses I chose to compare the MROS neurons only to units recorded in the exact same session in order to rule out that circumstantial conditions were responsible for the variability in OSI response to movement. The distribution of most MROS and OS units were skewed above the dashed line in the scatterplot which shows that the effect of movement on orientation selectivity was a reduced OSI (Figure 3.6). In the original cell population (n=232), 20 % of the OS units showed an increased OSI during movement recordings (Figure 3.6). However, there were no OS units with increased OSI during active behavior in the cell population recorded simultaneously with MROS neurons (n=120, Figure 3.8). This difference may either be due to properties of the recorded units or the cell layer, or it may be caused by different recording conditions in sessions where we did not find MROS neurons. Behavior in these sessions was not as strictly controlled as those including the MROS units, thus separation of sessile and movement recordings may not be as reliable. By restricting the analyses to the populations recorded simultaneously as MROS units, we demonstrate that the MROS phenotype was not a product of circumstantial conditions, as all three groups, the MROS, OS and OE neurons, were recorded in the same session and likely from the same microcircuits.

Sauvan (1999) observed that 40 % of the cells in V2/V3/V3A in monkey displayed orientation constancy and this could be true for the extrastriate cortex in rats as well. However, in a pilot experiment conducted in the mediolateral and lateral area of the secondary visual cortex of one rat we were unable to detect any MROS neurons. This could be because extrastriate cortex is organized differently in rats and monkeys and should be subject to future investigation.

4.3 Functional properties of MROS and simultaneously recorded units

Movement resistance in cortical neurons has been shown with regards to the change in angle of the preferred orientation during tilt (Sauvan, 1999). In the present study I also examine OSI and neuronal activity of MROS neurons during sessile and active behavior, and compare these features within and across different ensembles of neurons during both conditions.

4.3.1 Orientation Selectivity

The OSI was used as a measurement to quantify the unit's orientation selectivity. The results show that the OSI in all groups was significantly affected by movement, but the most dramatic effect was found in OS units with a 40 % reduction in OSI during movement. Our results suggest that MROS and OS units have similar orientation selectivity properties with regards to OSI during sessile behavior although the MROS units have a tendency towards higher OSIs. However, during movement the OSI is significantly reduced in OS units and often below the threshold of an OSI>0.45 to be considered orientation selective, while MROS units remain highly selective and sharply tuned in both conditions through some compensatory mechanism (Figure 3.9). Furthermore, the mean change in OSI from sessile to active behavior for OS cells was more than three times that of MROS and OE neurons and was significantly different between groups.

4.3.2 Evoked and spontaneous firing rates

Until recently, most studies in V1 were performed in anesthetized animals, although the neuronal activity has been shown to be much higher in awake animals (Fontanini & Katz, 2008; Greenberg et al., 2008; Livingstone et al., 1996). Furthermore, locomotion also increases the responses in V1 in head-fixed animals (Niell & Stryker, 2010; Keller et al., 2012). Even though it was not significant for all groups, we also observed a tendency towards increased firing rates from sessile to active behavior. The evoked and spontaneous firing rates during sessile recordings were significantly different across groups, but the same was not true for movement recordings (Figure 3.10). Furthermore, the MROS neurons showed a mean evoked rate in relation to the spontaneous rate that was twice as high as OS neurons, and

triple that seen in OE neurons. This evoked/spontaneous ratio was significantly different across groups, and did not seem to be affected by movement within groups.

The evoked firing rate is simply measured as the firing rate after onset of stimulus, which means that an increase in the overall firing rate, including spontaneous activity, will lead to a rise in the evoked firing rate as well. Despite not being statistically significant for all groups, there was a tendency towards increased evoked and spontaneous firing rates from sessile to moving behavior. However, the increase in evoked response in MROS neurons is specific for the unit's preferred orientation, whereas an increase in the visually evoked responses in OS or OE neurons was due to a non-specific increase in the overall firing rate (Figure 3.11).

This is also reflected in the OSI of MROS and OS units. Since the increase in evoked firing rate for MROS units is mostly specific for their preferred orientation it will not reduce the OSI much. In contrast, the increase in evoked firing rate for OS neurons during movement is non-specific, and will lead to a higher firing rate at all orientations. Since the OSI is calculated as (Rpref - Rorth) / (Rpref + Rorth), an increase in firing rates at directions orthogonal to the preferred orientation (Rorth) will reduce OSI in OS neurons, as is seen during movement. The significant increase in evoked rate observed for OS units was likely due to this non-specific increase in overall firing activity during movement. Recent work suggests that VIP positive inhibitory neurons may be responsible for the enhanced firing activity observed during movement (Fu et al., 2015). They observed that these neurons activate during movement, and that optogenetic activation of VIP positive inhibitory neurons in stationary animals mimicked the effect of locomotion on excitatory neurons. However, how the MROS neurons are kept highly selective during movement is yet to be established.

4.4 Tracer injections to reveal connectivity

There are many intriguing questions yet to be answered. What kind of compensatory input do the MROS neurons receive to make them stable, and where does it come from? Why are they kept stable, i.e. what is the role of these neurons? And lastly, what areas receive output from these MROS neurons and how are they affected? In this study we were unable to accurately answer these questions but the results raise interesting aspects for the functional implications of the MROS neurons for visual information processing.

4.4.1 Retrograde tracing using cholera toxin subunit B injection

One hypothesis is that the stability of the orientation tuning of the MROS units may play a role in compensatory mechanisms and modulate orientation tuning during movement. Since the MROS neurons were located mainly in L6, we wanted to further explore the feedback connection to the dLGN as this could be a pathway of modulating what input arrives in the cortex. We successfully labeled cortico-thalamic L6 neurons by a retrograde tracer injection in dLGN (Figure 3.13). The additional sparse labeling of L5 cortico-thalamic neurons indicate that the injection was too deep entering the vLGN where L5 neurons are known to project (Deschenes, 1994), as layer 5 does not project to the dLGN (Bourassa & Deschênes, 1995). Interestingly, we found that the majority of PCP4-expressing neurons in upper L6 co-localized with CTxB labeled neurons, whereas L5 cortico-thalamic cells did not. This is in accordance with Watakabe and co-workers (2012), in that PCP4 expressing neurons are reliable markers for deeper layers. This also reveals that the PCP4-expressing neurons in upper L6 are to a large extent cortico-thalamic as they co-localize with CTxB labeled neurons targeted by injection in the dLGN.

Recent studies in mice show that some dLGN neurons are direction- and orientation selective and it is suggested that direction selective retinal ganglion cells are the source of this tuning (Huberman et al., 2009; Marshel et al., 2012; Piscopo et al., 2013). The L6 receives direct input from the dLGN (Briggs & Usrey, 2007; Constantinople & Bruno, 2013) and recent findings indicate that the direct dLGN input to L6 may serve a different function compared to L4 input (L. Wang et al., 2013) but it is still unknown what type of dLGN neurons project to L6 and how this input affects the deep layer neurons. It is tempting to speculate that the MROS neurons could be the end-target of a specialized circuit for stimulus selectivity in the primary visual pathway, and receive direct input from orientation selective dLGN cells. However, as we did not investigate the connectivity of the MROS neurons we cannot know if they are cortico-thalamic or receive direct thalamo-cortical input. Nevertheless, the results indicate that the stereotaxic coordinates targeted the areas well and can, with minor adjustments, be used for future experiments. For instance, optogenetic manipulation of inputs or projection neurons should be used to further investigate the MROS neurons connectivity and function (see section 4.5).

4.4.2 Anterograde tracing with a viral vector

Recent studies have shown that L6 modulate neuronal activity in all cortical layers of V1 and the dLGN (Bortone et al., 2014; J. Kim et al., 2014; Olsen et al., 2012). We speculate that MROS neurons can be a baseline for visually induced cortical activity and that they are kept stable at all times to be able to execute this modulatory effect that have been observed. We do not know what areas are responsible for the stability of MROS units, but we wanted to further investigate where they project to and might be reciprocally connected to. Through the injection of an anterograde viral vector in L6, I found expression in the dLGN which again confirmed the feedback connection of V1 to LGN (Figure 3.14). In addition, the connections we observed to the nRT and LP are in accordance with previous studies of L6 projections (Bortone et al., 2014; Deschênes et al., 1994; Zarrinpar & Callaway, 2006).

As mentioned previously, it is likely that MROS neurons receive compensatory input from brain regions that are not part of the primary visual pathway. This may involve areas like the vestibular nuclei which are important for vestibulo-ocular and optokinetic reflexes, superior colliculus (SC) which is important for controlling eye movement or the posterior parietal cortex (PPC) which is known to play an important role in spatial aspects of vision. The V1 is indirectly or directly connected to all of these areas; the brainstem and SC through L5 (Bourassa & Deschênes, 1995; Deschênes et al., 1994; Scanziani, 2016; Tsiola et al., 2003) and the PPC through reciprocal connections with SC or reciprocal connection with LP which L5 and L6 are connected to (Bortone et al., 2014; Bourassa & Deschênes, 1995; Kamishina et al., 2009). It was beyond the scope of this study to examine projections to and from most of these areas but the viral injection confirms the projections from L6 to LP, which could transfer information from V1 to PPC outside the visual streams. The PPC is thought of as an end-point in the ventral stream, and it is also intriguing to speculate that MROS neurons might be kept stable through indirect input from PPC which has already been carefully processed in the visual pathway.

The viral vector used in this injection was carrying ChR2-GFP which in addition to being a tracer can be used for optogenetic manipulation. Importantly, the injection also confirms that the AAV5-syn-ChR2-GFP reliably labeling anterograde targets and lays the foundations for functional studies with optogenetic manipulations of connected brain regions. This approach can be used in future experiments to further explore the connectivity and functions of MROS

neurons perhaps by combining optogenetic stimulation of projection terminals and electrophysiological recordings of neural activity in the visual cortex.

4.5 Future perspectives

As the yield of MROS neurons was low, additional experiments are necessary to support the data of MROS neurons. The protocol used for recording the neurons was developed during the course of this work, and with the improvements made, new experiments should be conducted under more reproducible conditions. Improved tracking would also be an advantage in particular with regards to head movement and eye-movement, to assess what kind of movement is responsible for the stability and instability seen in MROS and OS neurons, respectively. In the protocol we established, we planned to anesthetize the animals when MROS neurons were detected to further investigate their properties. In a pilot experiment, the MROS neuron seemed to overcompensate for the head tilt, but from the limited recordings we acquired, we would not obtain conclusive results. In future experiments, the effect of head tilt on orientation selectivity in anesthetized animals will be included to the protocol. Furthermore, it is critical to investigate if MROS neurons have cortico-thalamic projections to the dLGN. One approach is to inject viral vectors into the dLGN together with an optic fiber and simultaneously do electrophysiological recordings from V1. When a MROS unit is located, optogenetic activation in dLGN of cortico-thalamic cells could then reveal if MROS neurons are projecting to the dLGN or not. The stereotaxic coordinates and use of viral vectors established in the current study can be used as a basis for such experiments.

4.6 Conclusions

Taken together, the results in this thesis suggest that all excitatory neurons in V1 are to some extent affected by self-movement, but unlike other cortical neurons, a subpopulation of deep layer movement resistant orientation selective (MROS) neurons remain highly selective to their preferred orientation. These neurons showed variable waveform, and did not seem to differ from other excitatory units in this regard. The MROS neurons are characterized by high OSI values during both sessile and active recordings, while the OSI of other orientation selective (OS) neurons is greatly reduced during movement.

Assessing the neuronal activity, we observed a tendency of increased firing rates during movement. The increase in evoked firing rate in MROS neurons was mostly confined to the unit's preferred orientation, and did not greatly affect tuning properties. In contrast, the increase in OS units' evoked firing rates was most likely due to an overall increase in neuronal activity which consequently reduced the OSI. We also observed that MROS neurons have a higher mean ratio of evoked rate in relation to spontaneous firing rate compared to other groups, and there was a significant difference in this ratio across groups for both movement and sessile behavior. Lastly we found that MROS neurons appear to be located in the deep cortical layers, mainly L6, which have been shown to have specialized functions in visual processing. The deep layers have intriguing connections in regard to MROS neurons, including direct and indirect connections to areas involved in visual processing, vestibular effects, and movement, and in this study we confirm projections to the dLGN, nRT and LP through tracer injections. These projections likely play a role in maintaining the stability of MROS neurons through compensatory input from for instance the PPC which is important for spatial aspects of vison and is reciprocally connected to the LP, or perhaps from vestibular areas important to the sense of balance and spatial orientation which is highly relevant as the MROS neurons are resistant to head and body movement.

The projections to and from V1, as well as intracortical excitatory and inhibitory networks, could all play a role in defining the stability of MROS neurons. Many different theories arise from their stable OSI and their location in the deep layers which exhibit several distinct connectivity patterns that suggest highly specialized functions. This opens for new experiments to dissect the underlying circuitry responsible for their remarkable firing patterns and their role for visual cortical processing. Moreover, these findings are essential to computational models that aim to understand visual information processing.

5 References

Ahmed, B., Anderson, J. C., Douglas, R. J., Martin, K. A. C., & Nelson, J. C. (1994). Polyneuronal innervation of spiny stellate neurons in cat visual cortex. *Journal of Comparative Neurology, 341*(1), 39-49.

Allen Brain Observatory (2016). Allen Mouse Brain Connectivity Atlas. *Allen Institute for Brain Science, http://connectivity.brain-map.org/*.

Allen Brain Observatory (2016). Technical Whitepaper: Stimulus Set and Response Analysis. *Allen Institute for Brain Science, http://www.brain-map.org/*.

Allison, J. D., Casagrande, V. A., & Bonds, A. B. (1995). The influence of input from the lower cortical layers on the orientation tuning of upper layer V1 cells in a primate. *Visual Neuroscience, 12*(2), 309-320.

Barbur, J. L., Watson, J. D. G., Frackowiak, R. S. J., & Zeki, S. (1993). Conscious visual perception without VI. *Brain: a Journal of Neurology, 116*(6)

Bartho, P., Hirase, H., Monconduit, L., Zugaro, M., Harris, K. D., & Buzsaki, G. (2004). Characterization of neocortical principal cells and interneurons by network interactions and extracellular features. *Journal of Neurophysiology, 92*(1), 600-608.

Bereshpolova, Y., Stoelzel, C. R., Zhuang, J., Amitai, Y., Alonso, J. M., & Swadlow, H. A. (2011). Getting drowsy? Alert/nonalert transitions and visual thalamocortical network dynamics. *Journal of Neuroscience,, 31*(48), 17480-17487.

Bolz, J., & Gilbert, C. D. (1986). Generation of end-inhibition in the visual cortex via interlaminar connections. *Nature, 320*(6060), 362-365.

Bortone, Dante S., Olsen, Shawn R., & Scanziani, M. (2014). Translaminar Inhibitory Cells Recruited by Layer 6 Corticothalamic Neurons Suppress Visual Cortex. *Neuron, 82*(2), 474-485.

Bourassa, J., & Deschenes, M. (1995). Corticothalamic projections from the primary visual cortex in rats: a single fiber study using biocytin as an anterograde tracer. *Neuroscience, 66*(2), 253-263.

Bourassa, J., & Deschênes, M. (1995). Corticothalamic projections from the primary visual cortex in rats: a single fiber study using biocytin as an anterograde tracer. *Neuroscience, 66*(2), 253-263.

Briggs, F., & Usrey, W. M. (2007). A Fast, Reciprocal Pathway between the Lateral Geniculate Nucleus and Visual Cortex in the Macaque Monkey. *Journal of Neuroscience, 27*(20), 5431-5436.

Bruno, R. M., & Simons, D. J. (2002). Feedforward mechanisms of excitatory and inhibitory cortical receptive fields. *Journal of Neuroscience, 22*(24), 10966-10975.

Buzsaki, G. (2004). Large-scale recording of neuronal ensembles. *Nature Neuroscience, 7*(5), 446-451.

Callaway, E. M. (1998). Local circuits in primary visual cortex of the macaque monkey. *Annual Review of Neuroscience, 21*, 47-74.

Chandler, H. C., King, V., Corwin, J. V., & Reep, R. L. (1992). Thalamocortical connections of rat posterior parietal cortex. *Neuroscience Letters, 143*(1-2), 237-242.

Chen, G., Rasch, M. J., Wang, R., & Zhang, X. H. (2015). Experience-dependent emergence of beta and gamma band oscillations in the primary visual cortex during the critical period. *Scentifici Reports, 5*, 17847.

Chung, S., & Ferster, D. (1998). Strength and orientation tuning of the thalamic input to simple cells revealed by electrically evoked cortical suppression. *Neuron, 20*(6), 1177-1189.

Constantinople, C. M., & Bruno, R. M. (2013). Deep cortical layers are activated directly by thalamus. *Science, 340*(6140), 1591-1594.

Conte, W. L., Kamishina, H., Corwin, J. V., & Reep, R. L. (2008). Topography in the projections of lateral posterior thalamus with cingulate and medial agranular cortex in relation to circuitry for directed attention and neglect. *Brain Research, 1240*, 87-95.

Crook, J. M., Kisvárday, Z. F., & Eysel, U. T. (1998). Evidence for a contribution of lateral inhibition to orientation tuning and direction selectivity in cat visual cortex: reversible inactivation of functionally characterized sites combined with neuroanatomical tracing techniques. *European Journal of Neuroscience, 10*(6), 2056-2075.

Cruz-Martin, A., El-Danaf, R. N., Osakada, F., Sriram, B., Dhande, O. S., Nguyen, P. L., . . . Huberman, A. D. (2014). A dedicated circuit links direction-selective retinal ganglion cells to the primary visual cortex. *Nature, 507*(7492), 358-361.

DeFelipe, J. (2011). The Evolution of the Brain, the Human Nature of Cortical Circuits, and Intellectual Creativity. *Frontiers in Neuroanatomy, 5*(29).

Denk, W., Strickler, J. H., & Webb, W. W. (1990). Two-photon laser scanning fluorescence microscopy. *Science, 248*(4951), 73-76.

Denney, D., & Adorjanti, C. (1972). Orientation specificity of visual cortical neurons after head tilt. *Experimental Brain Research, 14*(3), 312-317.

Deschênes, M., Bourassa, J., & Pinault, D. (1994). Corticothalamic projections from layer V cells in rat are collaterals of long-range corticofugal axons. *Brain Research, 664*(1–2), 215-219.

Ferguson, J. E., Boldt, C., & Redish, A. D. (2009). Creating low-impedance tetrodes by electroplating with additives. *Sensors and actuators. A, Physical, 156*(2), 388-393.

Fernandez, D. C., Chang, Y. T., Hattar, S., & Chen, S. K. (2016). Architecture of retinal projections to the central circadian pacemaker. *Proceedings of the National Academy of the USA, 113*(21), 6047-6052.

Fontanini, A., & Katz, D. B. (2008). Behavioral states, network states, and sensory response variability. *Journal of Neurophysiology, 100*(3), 1160-1168.

Fu, Y., Tucciarone, J. M., Espinosa, J. S., Sheng, N., Darcy, D. P., Nicoll, R. A., . . . Stryker, M. P. (2014). A cortical circuit for gain control by behavioral state. *Cell, 156*(6), 1139-1152.

Fyhn, M., Molden, S., Witter, M. P., Moser, E. I., & Moser, M. B. (2004). Spatial representation in the entorhinal cortex. *Science, 305*(5688), 1258-1264.

Gias, C., Hewson-Stoate, N., Jones, M., Johnston, D., Mayhew, J. E., & Coffey, P. J. (2005). Retinotopy within rat primary visual cortex using optical imaging. *Neuroimage, 24*(1), 200-206.

Gilbert, C. D., & Kelly, J. P. (1975). The projections of cells in different layers of the cat's visual cortex. *Journal of Comparative Neurology, 163*(1), 81-105.

Giolli, R. A., Blanks, R. H., & Lui, F. (2006). The accessory optic system: basic organization with an update on connectivity, neurochemistry, and function. *Progress in Brain Research, 151*, 407-440.

Girman, S. V., Sauve, Y., & Lund, R. D. (1999). Receptive field properties of single neurons in rat primary visual cortex. *Journal of Neurophysiology, 82*(1), 301-311.

Greenberg, D. S., Houweling, A. R., & Kerr, J. N. D. (2008). Population imaging of ongoing neuronal activity in the visual cortex of awake rats. *Nature neuroscience, 11*(7), 749-751.

Grieve, K. L., & Sillito, A. M. (1991a). The length summation properties of layer VI cells in the visual cortex and hypercomplex cell end zone inhibition. *Experimental Brain Research, 84*(2), 319-325.

Grieve, K. L., & Sillito, A. M. (1991b). A re-appraisal of the role of layer VI of the visual cortex in the generation of cortical end inhibition. *Experimental Brain Research, 87*(3), 521-529.

Guillery, R. W., & Sherman, S. M. (2002). Thalamic Relay Functions and Their Role in Corticocortical Communication: Generalizations from the Visual System. *Neuron, 33*(2), 163-175.

Hafting, T., Fyhn, M., Molden, S., Moser, M. B., & Moser, E. I. (2005). Microstructure of a spatial map in the entorhinal cortex. *Nature, 436*(7052), 801-806.

Han, Y., & Mrsic-Flogel, T. (2013). A finely tuned cortical amplifier. *Nature Neuroscience, 16*(9), 1166-1168.

Harrington, M. E. (1997). The ventral lateral geniculate nucleus and the intergeniculate leaflet: interrelated structures in the visual and circadian systems. *Neuroscience and Biobehavioral Reviews, 21*(5), 705-727.

Harris, K. D., & Shepherd, G. M. G. (2015). The neocortical circuit: themes and variations. *Nature Neuroscience, 18*(2), 170-181.

Hartline, H. K. (1941). The neural mechanisms of vision. *Harvey Lectures 37:39-68*.

Helmchen, F., Fee, M. S., Tank, D. W., & Denk, W. (2001). A Miniature Head-Mounted Two-Photon Microscope: High-Resolution Brain Imaging in Freely Moving Animals. *Neuron, 31*(6), 903-912.

Hubel, D. H., & Wiesel, T. N. (1959). Receptive fields of single neurones in the cat's striate cortex. *Journal of Physiology, 148*(3), 574-591.

Hubel, D. H., & Wiesel, T. N. (1962). Receptive fields, binocular interaction and functional architecture in the cat's visual cortex. *Journal of Physiology, 160*(1), 106-154.102.

Hubel, D. H., & Wiesel, T. N. (1974). Uniformity of monkey striate cortex: a parallel relationship between field size, scatter, and magnification factor. *Journal of Comparative Neurology, 158*(3), 295-305.

Huberman, A. D., Wei, W., Elstrott, J., Stafford, B. K., Feller, M. B., & Barres, B. A. (2009). Genetic Identification of an On-Off Direction- Selective Retinal Ganglion Cell Subtype Reveals a Layer-Specific Subcortical Map of Posterior Motion. *Neuron, 62*(3), 327-334.

Kamishina, H., Conte, W. L., Patel, S. S., Tai, R. J., Corwin, J. V., & Reep, R. L. (2009). Cortical connections of the rat lateral posterior thalamic nucleus. *Brain Research, 1264*, 39-56.

Kandel, E. R., Schwartz, J. H., Jessell, T. M., Siegelbaum, S. A., & Hudspeth, A. J. (2013). *Principles of Neural Science, 5th edition*. The McGraw-Hill Companies.

Keller, G. B., Bonhoeffer, T., & Hubener, M. (2012). Sensorimotor mismatch signals in primary visual cortex of the behaving mouse. *Neuron, 74*(5), 809-815.

Kerlin, A. M., Andermann, M. L., Berezovskii, V. K., & Reid, R. C. (2010). Broadly tuned response properties of diverse inhibitory neuron subtypes in mouse visual cortex. *Neuron, 67*(5), 858-871.

Kim, J., Matney, C. J., Blankenship, A., Hestrin, S., & Brown, S. P. (2014). Layer 6 Corticothalamic Neurons Activate a Cortical Output Layer, Layer 5a. *The Journal of Neuroscience, 34*(29), 9656-9664.

Kim, T., & Freeman, R. D. (2016). Direction selectivity of neurons in the visual cortex is non-linear and lamina-dependent. *European Journal of Neuroscience, 43*(10), 1389-1399.

Kuffler, S. W. (1953). Discharge patterns and functional organization of mammalian retina. *Journal of Neurophysiology, 16*(1), 37-68.

Latawiec, D., Martin, K. A., & Meskenaite, V. (2000). Termination of the geniculocortical projection in the striate cortex of macaque monkey: a quantitative immunoelectron microscopic study. *Journal of Comparative Neurology, 419*(3), 306-319.

Lee, C. C., & Sherman, S. M. (2009). Modulator Property of the Intrinsic Cortical Projection from Layer 6 to Layer 4. *Frontiers in Systems Neuroscience, 3*, 3.

Lee, S.-H., Kwan, A. C., Zhang, S., Phoumthipphavong, V., Flannery, J. G., Masmanidis, S. C., . . . Dan, Y. (2012). Activation of Specific Interneurons Improves V1 Feature Selectivity and Visual Perception. *Nature, 488*(7411), 379-383.

Li, Y. T., Ibrahim, L. A., Liu, B. H., Zhang, L. I., & Tao, H. W. (2013). Linear transformation of thalamocortical input by intracortical excitation. *Nature Neuroscience, 16*(9), 1324-1330.

Lien, A. D., & Scanziani, M. (2013). Tuned thalamic excitation is amplified by visual cortical circuits. *Nature Neuroscience, 16*(9), 1315-1323.

Liu, B.-h., Li, Y.-t., Ma, W.-p., Pan, C.-j., Zhang, L. I., & Tao, H. W. (2011). Broad Inhibition Sharpens Orientation Selectivity By Expanding Input Dynamic Range in Mouse Simple Cells. *Neuron, 71*(3), 542-554.

Livingstone, M. S., Freeman, D. C., & Hubel, D. H. (1996). Visual responses in V1 of freely viewing monkeys. *Cold Spring Harbor Symposia on Quantitative Biology, 61*, 27-37.

Markram, H., Toledo-Rodriguez, M., Wang, Y., Gupta, A., Silberberg, G., & Wu, C. (2004). Interneurons of the neocortical inhibitory system. *Nature Reviews Neuroscience, 5*(10), 793-807.

Marshel, J., Kaye, A., Nauhaus, I., & Callaway, E. (2012). Anterior-Posterior Direction Opponency in the Superficial Mouse Lateral Geniculate Nucleus. *Neuron, 76*(4), 713-720.

Martinez, L. M., Wang, Q., Clay Reid, R., Pillai, C., Alonso, J.-M., Sommer, F. T., & Hirsch, J. A. (2005). Receptive field structure varies with layer in the primary visual cortex. *Nature neuroscience, 8*(3), 372-379.

Niell, C. M. (2013). Vision: More Than Expected in the Early Visual System. *Current Biology, 23*(16), R681-R684.

Niell, C. M., & Stryker, M. P. (2008). Highly Selective Receptive Fields in Mouse Visual Cortex. *Journal of Neuroscience,, 28*(30),

Niell, C. M., & Stryker, M. P. (2010). Modulation of Visual Responses by Behavioral State in Mouse Visual Cortex. *Neuron, 65*(4), 472-479.

O'Keefe, J., & Dostrovsky, J. (1971). The hippocampus as a spatial map. Preliminary evidence from unit activity in the freely-moving rat. *Brain Research, 34*(1), 171-175.

Olsen, S. R., Bortone, D. S., Adesnik, H., & Scanziani, M. (2012). Gain control by layer six in cortical circuits of vision. *Nature, 483*(7387), 47-52.

Paxinos, G., & Watson, C. (2007). *The rat brain in stereotaxic coordinates*. Amsterdam; Boston: Elsevier.

Peters, A., & Feldman, M. L. (1976). The projection of the lateral geniculate nucleus to area 17 of the rat cerebral cortex. I. General description. *Journal of Neurocytology, 5*(1), 63-84.

Petruno, S. K., Clark, R. E., & Reinagel, P. (2013). Evidence that primary visual cortex is required for image, orientation, and motion discrimination by rats. *Public Library of Science one, 8*(2), e56543.

Piscopo, D. M., El-Danaf, R. N., Huberman, A. D., & Niell, C. M. (2013). Diverse visual features encoded in mouse lateral geniculate nucleus. *Journal of Neuroscience, 33*(11), 4642-4656.

Priebe, N. J., & McGee, A. W. (2014). Mouse vision as a gateway for understanding how experience shapes neural circuits. *Frontiers in Neural Circuits, 8*, 123.

Purves, D., Augustine, G. J., Fitzpatrick, D., Hall, W. C., LaMantia, A.-S., & White, L. E. (2012). *Neuroscience, 5th edition*. Sunderland, Mass.: Sinauer Associates.

Reinhold, K., Lien, A. D., & Scanziani, M. (2015). Distinct recurrent versus afferent dynamics in cortical visual processing. *Nature Neuroscience, 18*(12), 1789-1797.

Reynolds, J. H., & Heeger, D. J. (2009). The Normalization Model of Attention. *Neuron, 61*(2), 168-185.

Sauvan, X. M. (1999). Orientation Constancy in Neurons of Monkey Visual Cortex. *Visual Cognition, 6*(1), 43-54.

Sawinski, J., Wallace, D. J., Greenberg, D. S., Grossmann, S., Denk, W., & Kerr, J. N. (2009). Visually evoked activity in cortical cells imaged in freely moving animals. *Proceedings of the National Academy of Science of the USA, 106*(46), 19557-19562.

Scalia, F., & Arango, V. (1979). Topographic organization of the projections of the retina to the pretectal region in the rat. *Journal of Comparative Neurology, 186*(2), 271-292.

Scanziani, M. (2016). Adaptive Control of an Innate Reflex by Visual Cortex (Abstract) *FENS forum of Neuroscience 2016 (Abstract number S19B).*

Scholl, B., Tan, A. Y., Corey, J., & Priebe, N. J. (2013). Emergence of orientation selectivity in the Mammalian visual pathway. *Journal of Neuroscience, 33*(26), 10616-10624.

Shai, A. S., Anastassiou, C. A., Larkum, M. E., & Koch, C. (2015). Physiology of Layer 5 Pyramidal Neurons in Mouse Primary Visual Cortex: Coincidence Detection through Bursting. *Public Library of Science Computter Biology, 11*(3), e1004090.

Shapley, R., Hawken, M., & Ringach, D. L. (2003). Dynamics of Orientation Selectivity in the Primary Visual Cortex and the Importance of Cortical Inhibition. *Neuron, 38*(5), 689-699.

Sillito, A. M., Cudeiro, J., & Jones, H. E. (2006). Always returning: feedback and sensory processing in visual cortex and thalamus. *Trends in Neuroscience, 29*(6), 307-316.

Taube, J. S., Muller, R. U., & Ranck, J. B., Jr. (1990). Head-direction cells recorded from the postsubiculum in freely moving rats. I. Description and quantitative analysis. *Jorunal of Neuroscience, 10*(2), 420-435.

Thomson, A. M. (2010). Neocortical Layer 6, A Review. *Frontiers in Neuroanatomy, 4*, 13.

Tsiola, A., Hamzei-Sichani, F., Peterlin, Z., & Yuste, R. (2003). Quantitative morphologic classification of layer 5 neurons from mouse primary visual cortex. *Journal of Comparative Neurology, 461*(4), 415-428.

Van Horn, S. C., Erişir, A., & Sherman, S. M. (2000). Relative distribution of synapses in the A-laminae of the lateral geniculate nucleus of the cat. *Journal of Comparative Neurology, 416*(4), 509-520.

Velez-Fort, M., Rousseau, C. V., Niedworok, C. J., Wickersham, I. R., Rancz, E. A., Brown, A. P., . . . Margrie, T. W. (2014). The stimulus selectivity and connectivity of layer six principal cells reveals cortical microcircuits underlying visual processing. *Neuron, 83*(6), 1431-1443.

Wallace, D. J., Greenberg, D. S., Sawinski, J., Rulla, S., Notaro, G., & Kerr, J. N. (2013). Rats maintain an overhead binocular field at the expense of constant fusion. *Nature, 498*(7452), 65-69.

Wang, L., Kloc, M., Gu, Y., Ge, S., & Maffei, A. (2013). Layer-specific experience-dependent rewiring of thalamocortical circuits. *Journal of Neuroscience, 33*(9), 4181-4191.

Wang, L., Sarnaik, R., Rangarajan, K., Liu, X., & Cang, J. (2010). Visual receptive field properties of neurons in the superficial superior colliculus of the mouse. *Journal of Neuroscience, 30*(49), 16573-16584.

Wang, Q., & Burkhalter, A. (2007). Area map of mouse visual cortex. *Journal of Comparative Neurology, 502*(3), 339-357.

Wang, X., Chen, C., Zhang, D., & Yao, H. (2014). Cumulative latency advance underlies fast visual processing in desynchronized brain state. *Proceedings of the National Academy of Science of the USA, 111*(1), 515-520.

Watakabe, A., Hirokawa, J., Ichinohe, N., Ohsawa, S., Kaneko, T., Rockland, K. S., & Yamamori, T. (2012). Area-specific substratification of deep layer neurons in the rat cortex. *Journal of Comparative Neurology, 520*(16), 3553-3573.

Wilson, N. R., Runyan, C. A., Wang, F. L., & Sur, M. (2012). Division and subtraction by distinct cortical inhibitory networks in vivo. *Nature, 488*(7411), 343-348.

Yang, W., Carrasquillo, Y., Hooks, B. M., Nerbonne, J. M., & Burkhalter, A. (2013). Distinct Balance of Excitation and Inhibition in an Interareal Feedforward and Feedback Circuit of Mouse Visual Cortex. *Journal of Neuroscience, 33*(44), 17373-17384.

Zarrinpar, A., & Callaway, E. M. (2006). Local Connections to Specific Types of Layer 6 Neurons in the Rat Visual Cortex. *Journal of Neurophysiology, 95*(3), 1751-1761.

Zhang, H. Y., & Hoffmann, K. P. (1993). Retinal projections to the pretectum, accessory optic system and superior colliculus in pigmented and albino ferrets. *European Journal of Neuroscience, 5*(5), 486-500.

Zhao, X., Chen, H., Liu, X., & Cang, J. (2013). Orientation-selective Responses in the Mouse Lateral Geniculate Nucleus. *Journal of Neuroscience, 33*(31), 12751-12763.

6 Appendix

6.1 List of abbreviations

AP	anterioposterior
AVV-Syn	adeno-associated virus under synapsin promoter (carrying ChR2-GFP)
ChR2-GFP	Channelrhodopsin 2 with green fluorescent protein tag
CTxB	Cholera Toxin subunit B
dLGN	dorsal lateral geniculate nucleus
DV	dorsoventral
L1-L6	layer 1 to layer 6
LD	lateral dorsal nucleus
LFP	local field potentials
LP	lateral posterior nucleus
MROS	movement resistant orientation selective (neurons)
nRT	reticular thalamic nucleus
OE	other excitatory (neurons)
OS	orientation selective (neurons)
OSI	orientation selectivity index
PCP4	purkinje cell protein 4
PFA	paraformaldehyde
PPC	prefrontal parietal cortex
R	firing rate
SC	superior colliculus
SEM	standard error of the mean
V1	primary visual cortex
VIP	vasointestinal peptide (- positive inhibitory neurons)

6.2 Solutions used for immunohistochemistry and histochemistry

10 x PBS

80g of NaCl

2.0g of KCl

14.4g of Na2HPO4

2.4g of KH2PO4

Dissolve in 800 ml dH2O, adjust pH to 7.4, and adjust volume to 1L

Dilute 1:10 with dH2O for 1X solution

4% Paraformaldehyde (PFA)

40 g PFA

1 L 1X PBS

Heat to 50-60°C, leave with stirring until everything is dissolved (3-4 hours)

Filter before use

Cresyl violet staining solution

0.5 g cresyl violet acetate

1.25 mL glacial acetic acid

500 mL dH20

Heat to 60°C and filter before use

96% ethanol with acetic acid

500 mL absolute ethanol

2.5 mL acetic acid

6.3 Immunohistochemistry and histochemistry protocols

6.3.1 Staining of (AAV5-syn-) ChR2-GFP

Primary antibody: rabbit anti-GFP (A11122, Life Technologies)

Secondary antibody: goat anti-rabbit Alexa 488 (A11034, Life Technologies)

Blocking solution: 1% BSA, 0.03% Triton x-100 in 1xPBS

1. Rinse sections 3x5 min in 1xPBS
2. Block sections for 1 hour, room temp.
3. Incubate sections with primary antibody (1:1000) in block overnight, room temp.
4. Rinse sections 3x5 min in 1xPBS
5. Incubate sections with secondary antibody (1:1000) in 1xPBS for 2 hours, room temp.
6. Rinse sections 3x5min in 1xPBS
7. Mount sections, leave to dry
8. Rinse in ddH_2O, leave to dry
9. Add Fluorsave and coverglass

6.3.2 Staining of PCP4

Primary antibody: rabbit anti-PCP4 (HPA005792, Sigma-Aldrich)

Secondary antibody: goat anti-rabbit Alexa488 (A11034, Life Technologies)

Blocking solution: 1% BSA, 0.03% Triton x-100 in 1xPBS

1. Rinse sections 3x5 min in 1xPBS
2. Block sections for 1 hour, room temp.
3. Incubate sections with primary antibody (1:400) in block overnight, room temp.
4. Rinse sections 3x5 min in 1x PBS
5. Incubate sections with secondary antibody (1:400) in 1xPBS for 2 hours
6. Rinse sections 3x5 minutes in 1xPBS, mount sections, leave to dry
7. Rinse sections in ddH2O, leave to dry
8. Add Floursave and coverglass

6.3.3 Dual fluorescent staining of PCP4 and Nissl

Primary antibody: rabbit anti-PCP4 (HPA005792, Sigma-Aldrich)

Secondary antibody: goat anti-rabbit Alexa488 (A11034, Life Technologies)

Blocking solution: 1% BSA, 0.03% Triton x-100 in 1xPBS

1. Rinse sections 3x5 min in 1xPBS
2. Block sections for 1 hour, room temp.
3. Incubate sections with primary antibody (1:400) in block overnight, room temp.
4. Rinse sections 3x5 min in 1x PBS
5. Incubate sections with secondary antibody (1:400) in 1xPBS for 2 hours
6. Rinse sections 3x5 minutes in 1xPBS
7. Incubate in NeuroTrace Fluorescent Nissl Stain (1:100) diluted in 1xPBS for 30 min at room temp.
8. Incubate in 0.1 % Triton X-100 PBS for 10 min at room temp.
9. Rinse sections 2x5 min in 1xPBS, mount sections, leave to dry
10. Rinse sections in ddH2O, leave to dry
11. Add Floursave and coverglass

6.3.4 Nissl staining with cresyl violet

1. Immerse dry sections in a 1:1 chloroform: 100 % ethanol solution overnight in the fume hood, in order to secure sections to the glass slide
2. Hydrate the sections by immersing in
    a. 100 % ethanol for 2 min
    b. 90 % ethanol for 2 min
    c. 80 % ethanol for 2 min
    d. 70 % ethanol for 2 min
    e. dH2O for 2 min
3. Immerse the sections in cresyl violet solution for 6-10 min
4. Dehydrate the sections by immersing in
    a. dH2O for 2 min
    b. 70 % ethanol for 2 min
    c. 80 % ethanol for 2 min
    d. 90 % ethanol for 2 min
    e. 96 % ethanol with acetic acid for 1-5 min depending on the color fading
    f. 100 % ethanol for 2 min
    g. Xylene for 5-15 min
5. Cover with Entellan and a coverglass.
6. Leave in fume hood overnight to dry

6.4 Tuning curves and raster plots of MROS neurons

A)

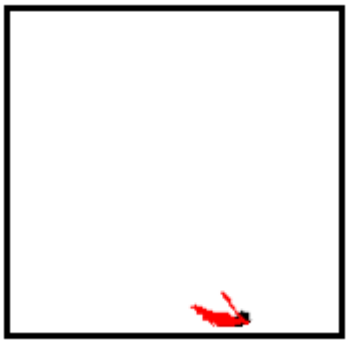

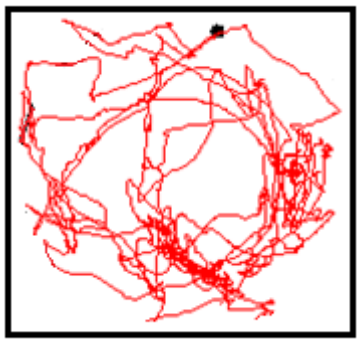

Cell 1, sessile session, OSI=1.00

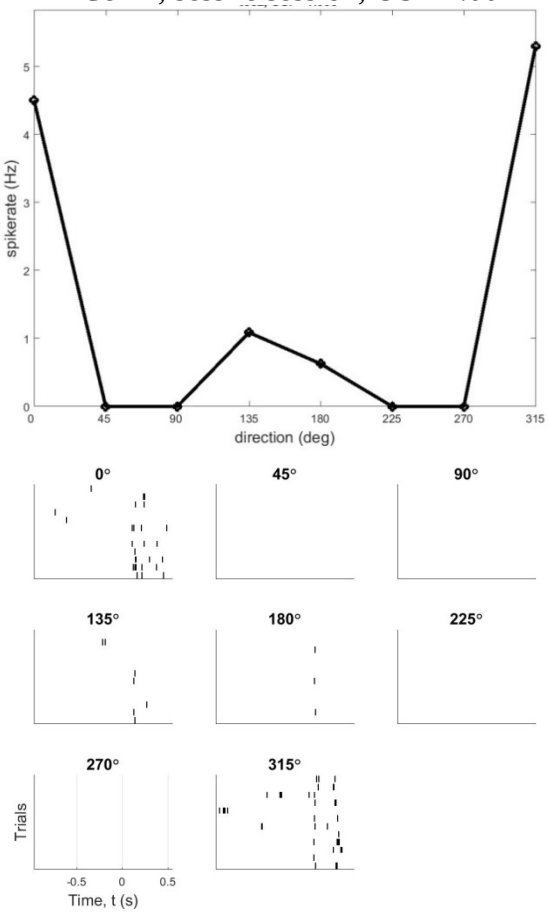

Cell 1, active session, OSI=0.892

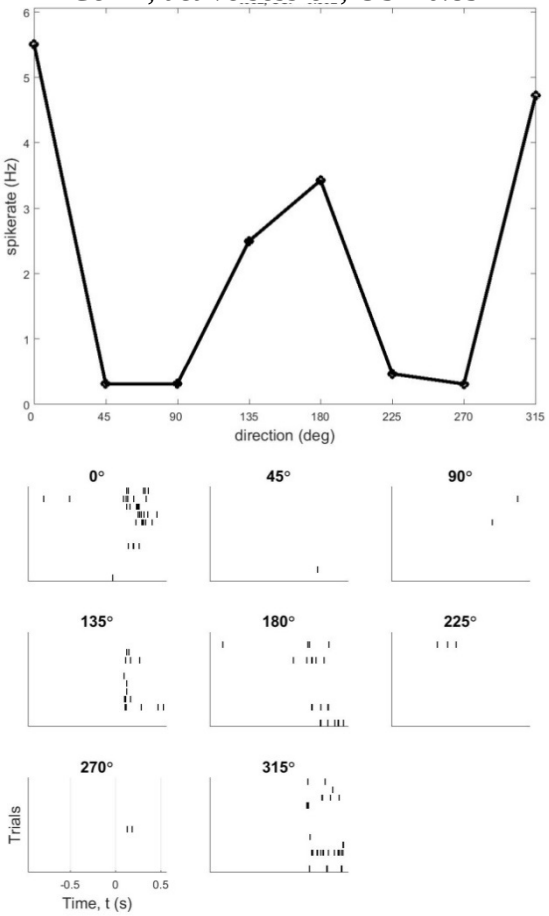

B)

Cell 2, sessile session, OSI=0.905

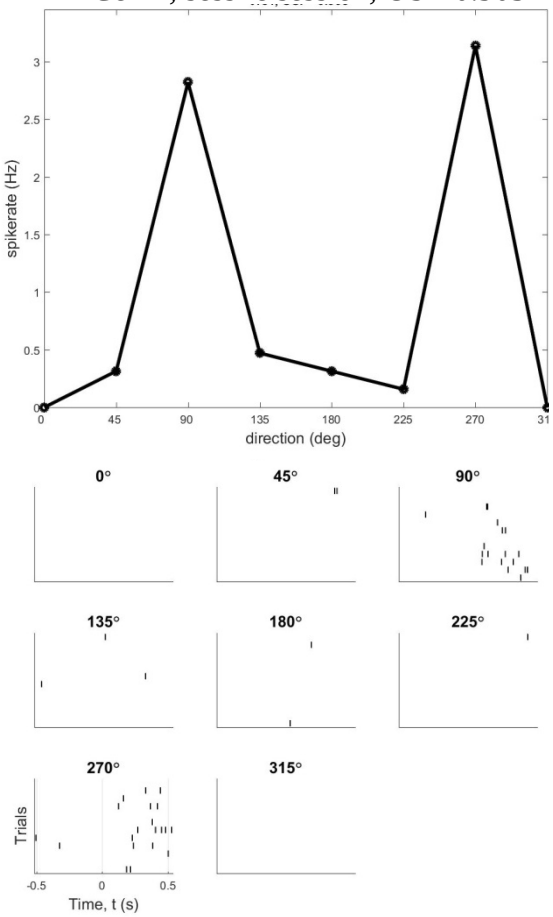

Cell 2, active session, OSI=0.949

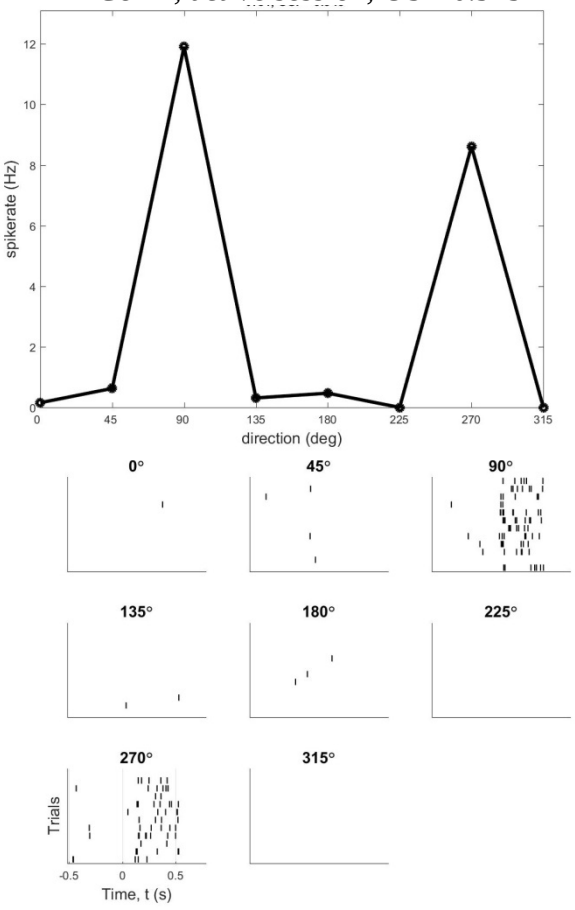

C)

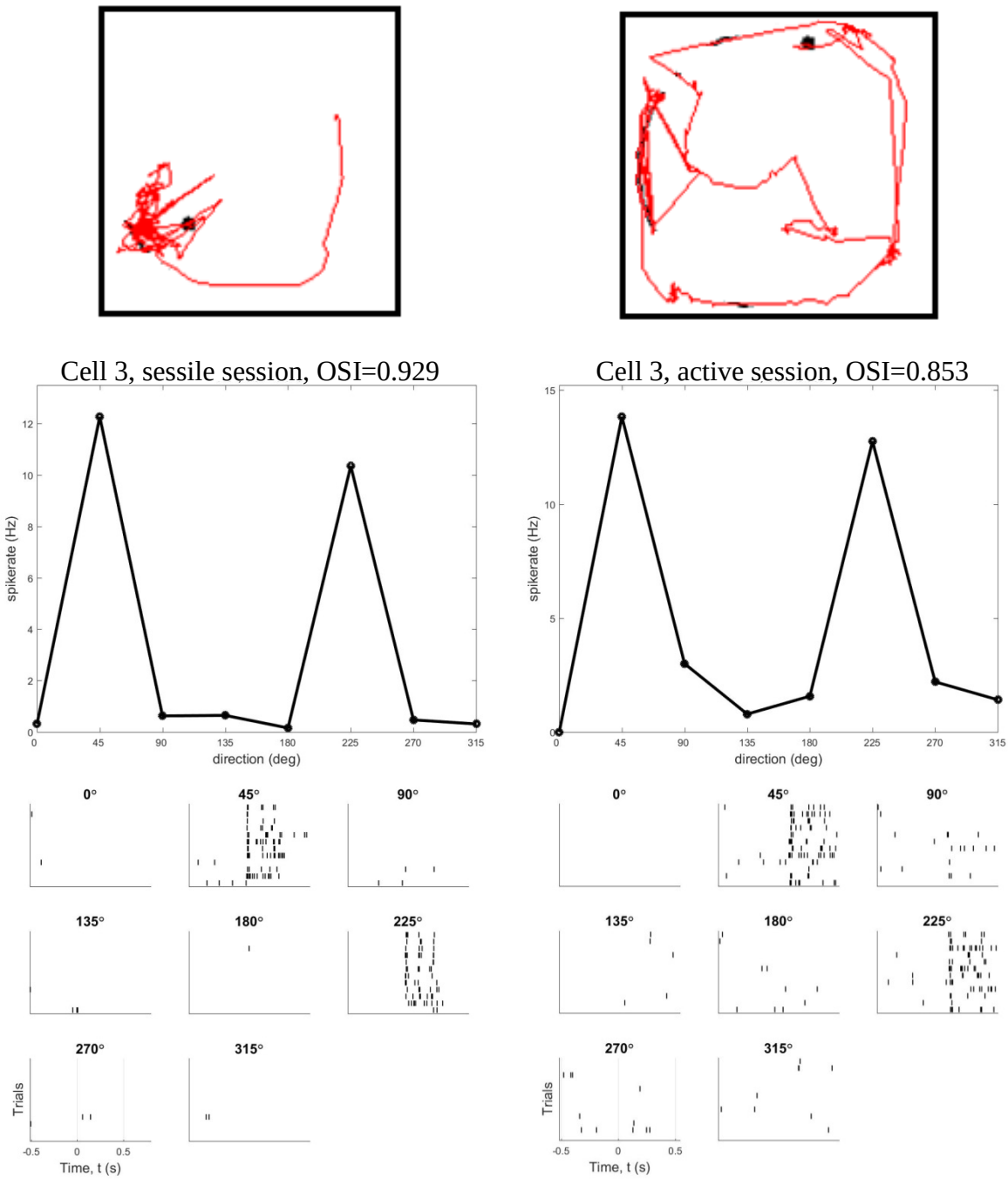
Cell 3, sessile session, OSI=0.929
Cell 3, active session, OSI=0.853
spikerate (Hz)
direction (deg)
0°
45°
90°
135°
180°
225°
270°
315°
Trials
Time, t (s)

D)

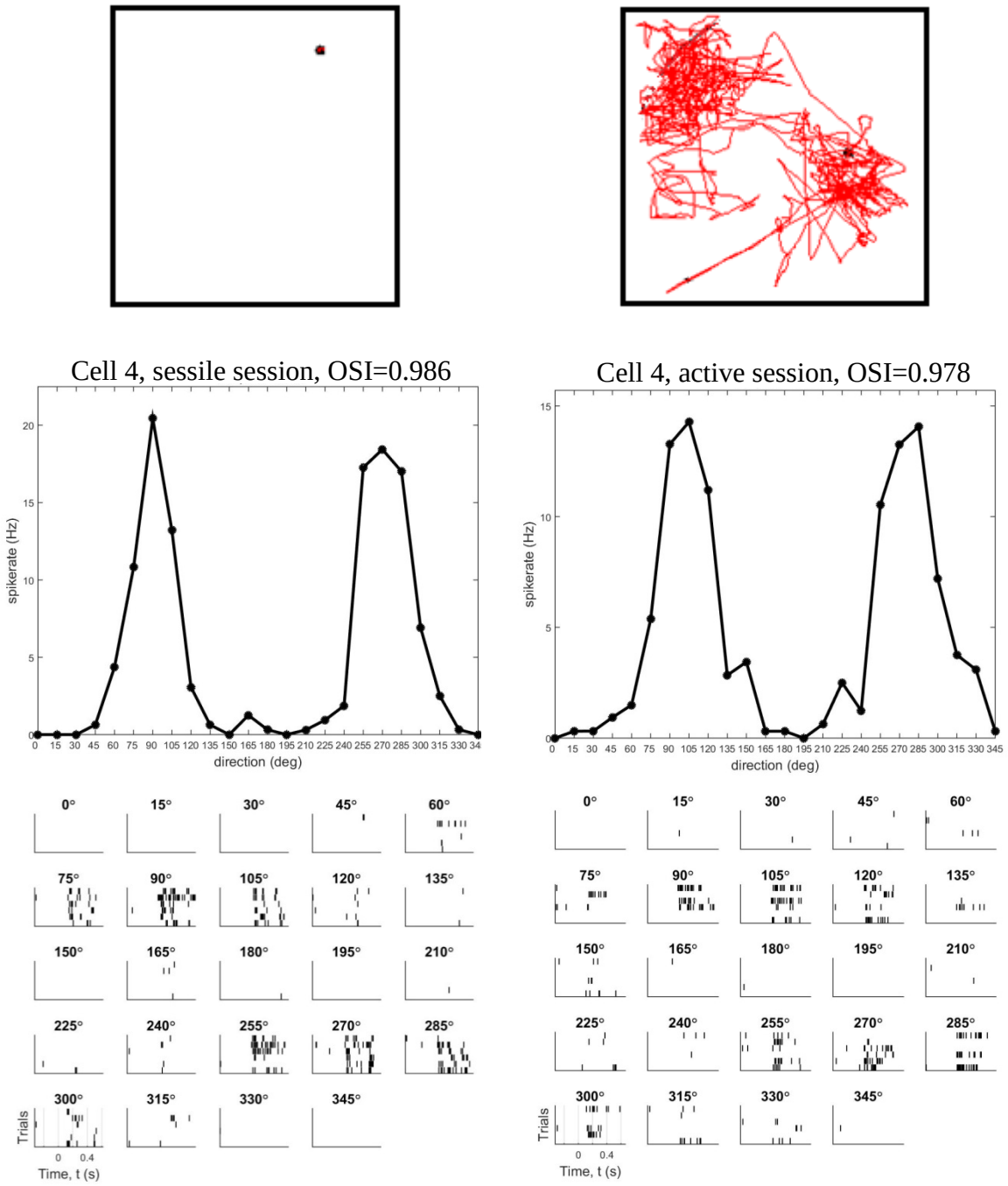

Figure 6.1: Trajectory plots (top panel), tuning curves (middle panel) and raster plots (bottom panel) for some MROS neurons demonstrating their remarkably stable orientation tuning during sessile (left panels) and active (right panels) behavior. A) Cell 1 responds to vertical gratings moving right (0˚) or left (180˚) on the screen. B) Cell 2 responds to horizontal gratings moving up (90˚) or downwards (270˚) on the screen C) Cell 3 responds to gratings moving diagonally (45˚/225˚) on the screen. D) Cell 4 has same response as cell 2, but recorded with 24 different orientations, 6 repetitions. A-C): 8 orientations, 12 repetitions.

6.5 Tetrode tracks

A)

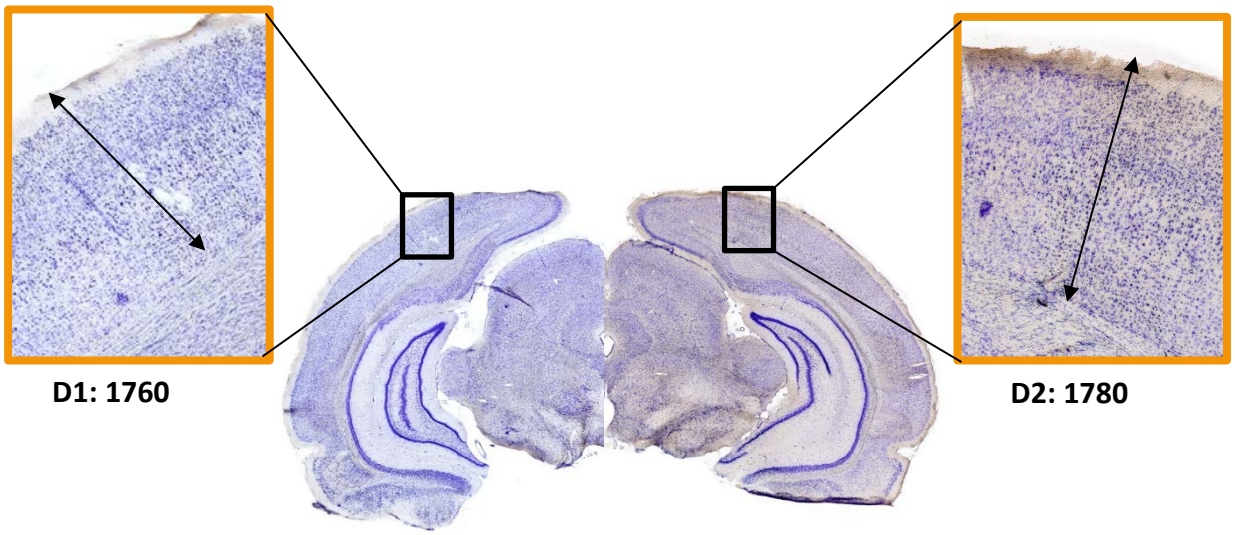

B)

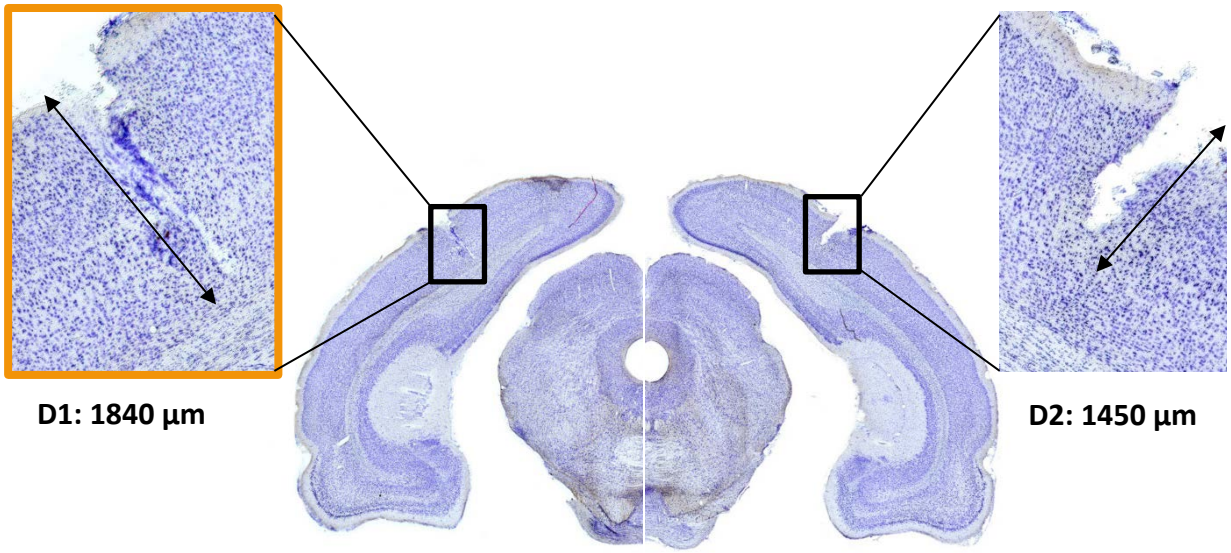

C)

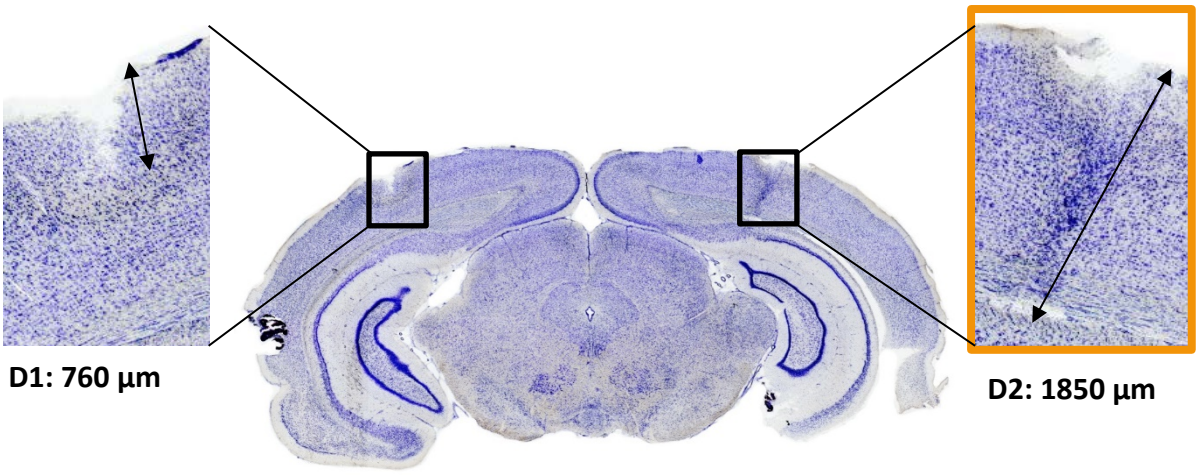

D)

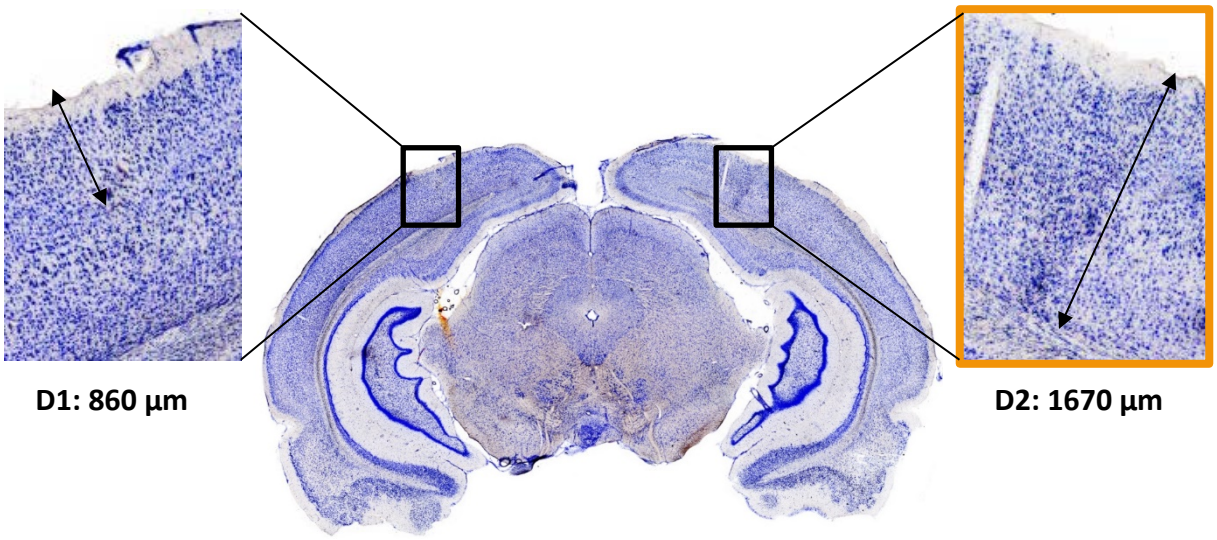

Figure 6.2: Tetrode tracks in the primary visual cortex (V1) of the four animals from which the 232 neurons used in analyses were recorded from. A-D) Coronal sections stained for Nissl bodies to visualize the tetrode track (left and right panels). Boxes enclosed in orange show traces of tetrodes where the movement resistant orientation selective (MROS) units were recorded. An estimated shrinkage of 15 % was taken into account for the tetrode depths (D1/D2) under left and right panels.